THE PROCEEDINGS OF
THE PHYSICAL SOCIETY

Section A

VOL. 62, PART 10 1 October 1949 No. 358 A

On the Ratio of Positive to Negative Particles in the Vertical Cosmic-Ray Beam at Sea Level

BY B. G. OWEN AND J. G. WILSON
The Physical Laboratories, University of Manchester

Communicated by P. M. S. Blackett; MS. received 4th April 1949.

ABSTRACT. A method of direct momentum measurement has been used to determine the ratio of positive to negative particles in the cosmic-ray beam at sea level. Measurements on about 12,000 particles give the ratio $+/-=1{\cdot}268\pm0{\cdot}023$, and it is further shown that to the statistical accuracy of the experiment there is no variation of this ratio with momentum over the momentum range 10^9–10^{10} ev/c.

§1. INTRODUCTION

MEASUREMENTS of the positive excess of energetic cosmic-ray particles, substantially of the meson component, hitherto reported are of two kinds. Blackett (1937), Jones (1939) and Hughes (1940) photographed cloud chamber tracks of single cosmic-ray particles in a magnetic field, and their results give very direct information for the range of momentum which is accepted by the chamber and its associated control and which is measurable in the particular conditions of experiment. However, the technique of accurate measurement of curvature is laborious, and the total number of tracks measured by each of these workers was only of the order of a thousand, a number sufficient to establish the existence of an excess of positive particles, although only within wide limits, but not large enough to yield significant results for separated ranges of momentum.

A different technique, initiated by Bernardini and his co-workers (1941) using a "lens" of magnetized iron has, more recently, been widely used. The results obtained by this method are not susceptible of the same direct interpretation as is possible for the cloud chamber method, for the apparatus becomes unselective at high momenta and has an efficiency of reception varying over the whole spectrum which is a function not only of simple geometry but also of the scattering of the particles traversing the magnetized iron blocks which form the lens. On the other hand the method has the high counting rate and portability which make it particularly suitable for relative measurements, provided that the particle spectrum at the various conditions of observation is sufficiently known.

The new magnetic spectrograph at Manchester University has made possible measurements comparable to those previously obtained in the cloud chamber at a very much accelerated collection rate. We give here an absolute value of the ratio of positive to negative particles, over a defined angle of collection and momentum spectrum, of considerably greater statistical weight than the early measurements, and we give also some preliminary indication of this ratio as a function of momentum.

§2. THE APPARATUS

A detailed description of the spectrograph and its operation will be given elsewhere. The magnetic deflection of particles canalized through the field gap of two large electromagnets (field 12,000 gauss, pole area 30 cm. × 40 cm., gap 10 cm.) is detected in three rows of Geiger counters, respectively above the upper magnet, between the magnets and below the lower magnet (see Plate). The length of path between the extreme counter rows is 5 m. The individual counters of the three rows are connected to neon lamps, and, on every occasion when a master selection condition is fulfilled, the lamps corresponding to the particular counters discharged flash and are photographed, thus defining the trajectory and deflection of the particle traversing the system. For the work now described the momentum of cosmic-ray particles near the vertical direction is measured with a "maximum detectable momentum" up to about 3×10^{10} ev/c. at a rate varying between 250 and 450 particles per day according to the condition of operation. The precision of measurement quoted is for operation with full magnetic field; in work referred to below with "low field" the corresponding maximum detectable momentum is $1{\cdot}5 \times 10^{10}$ ev/c.

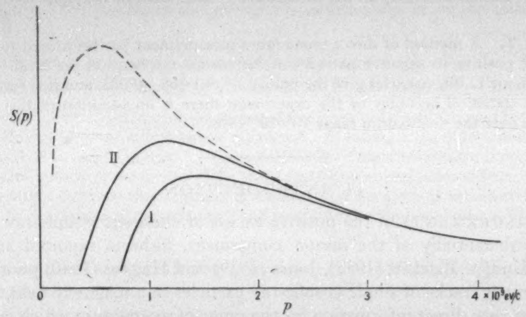

Figure 1. Momentum spectrum included in the determination of the ratio of positive and negative particles.
I—Measurements with high field. II—Measurements with low field.
Broken line—Meson sea-level spectrum according to Rossi (1948).

The momentum spectrum and angular collection for which our measurements are made are shown in Figures 1 and 2. For comparison with the momentum spectrum of the particles actually used in our determination, the sea-level spectrum of mesons adopted by Rossi (1948) is also given in Figure 1. It is apparent that our measurements, of which the greater part were made with the lower value of magnetic field, give virtually no information about very slow mesons ($p \lesssim 5 \times 10^8$ ev/c.); all of the other experiments to which we have referred show a similar bias against slow mesons.

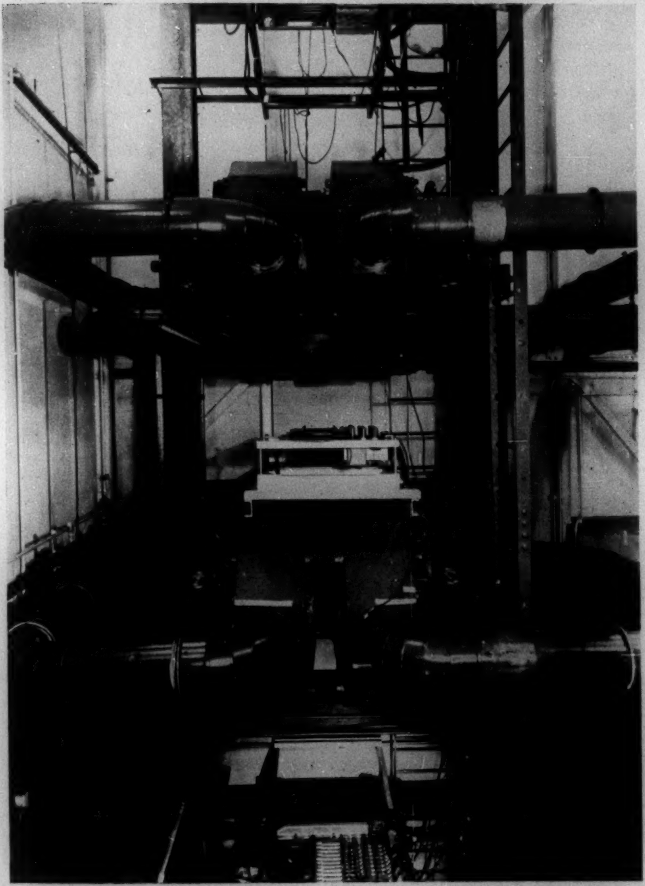

Magnetic spectrograph, general view.

In Figure 2 the angular collection of the spectrograph is shown as a function of particle momentum, and it must be noted that the values of the positive–negative ratio given (Table 2) as a function of momentum refer to different collecting directions, a feature which applies also to the other measurements quoted. Our method of measurement in fact defines the direction of every incident trajectory to about ±1°, and hence, were enough data available, a comparison of the ratio for different momenta in similar directions of collection could be made.

§3. RESULTS

Measurements were made of groups of approximately 3,000 tracks. This number was chosen in the first instance to correspond to a weekly reversal of the deflecting field, and the first group in fact consisted of successive runs of about 1,500 tracks between which the field was reversed. For later groups a daily reversal of deflecting field was adopted, but for convenience groups of approximately 3,000 tracks were still collected.

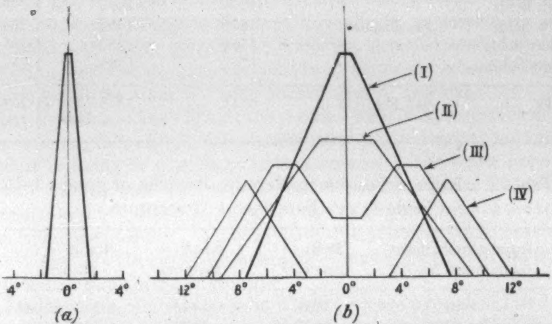

Figure 2. Angular collection of spectrograph (*a*) in E–W plane, (*b*) in N–S plane. (*b*, i) undeviated particles ; (*b*, ii) 4×10^9 ev/c. in high field, 2×10^9 ev/c. in low field; (*b*, iii) 2×10^9 ev/c. in high field, 10^9 ev/c. in low field; (*b*, iv) $1{\cdot}3\times10^9$ ev/c. in high field, $0{\cdot}7\times10^9$ ev/c. in low field.

The results for four groups of tracks are given in Table 1 in which are also summarized the results of cloud chamber measurements. The momentum ranges to which the results quoted for cloud chamber measurements apply are given, since particles of low momentum ($p<5\times10^8$ ev/c.) recorded by Blackett (1937) and by Hughes (1940) have been rejected because of the uncertain number of electrons which are involved in these groups. Hughes measured two groups of tracks for one of which the particles, after traversing the cloud chamber, passed through 10 cm. of lead, but obtained no significant difference in the results; these groups have accordingly been combined. The statistical standard error of the ratio +/− is given in each instance.

In Table 2 and in Figure 3 our results are shown as a function of particle momentum. Since any variation with momentum of the ratio of positive to negative particles is certainly not large compared with the statistical uncertainty of the various measurements, the mean momentum of each group has not been determined with great precision.

The particles in the group of mean momentum about 10^{10} ev/c. include the particles of highest momentum for which a deflection of trajectory can be recorded. The actual distribution of momentum in this group will be discussed elsewhere,

Table 1. The Ratio of Positive to Negative Particles

Workers	Momentum range	Positive particles	Negative particles	Ratio +/− particles
Blackett (1937)	$p>5\times10^8$ ev/c.	393	336	1·17±0·09
Jones (1939)	$p>2\times10^8$ ev/c.	416	323	1·29±0·10
Hughes (1940)	$p>5\times10^8$ ev/c.	595	487	1·22±0·08
O. & W. (1949)				
I (high field)		1575	1232	1·278±0·049
II (low field)	See Figure 1	1836	1468	1·251±0·044
III (low field)		1569	1250	1·255±0·048
IV (low field)		1763	1385	1·273±0·046
Total I–IV	See Figure 1	6743	5335	(1·264) 1·268±0·023

Table 2. Ratio of Positive to Negative Particles of groups I–IV (Table 1) as a Function of Momentum

Approximate mean momentum (ev/c.)	Positive particles	Negative particles	Ratio +/− particles
10^9	1781	1430	1·247±0·044
2×10^9	1927	1455	1·324±0·046
4×10^9	1461	1180	1·238±0·048
10^{10}	1576	1276	(1·235) 1·252±0·046

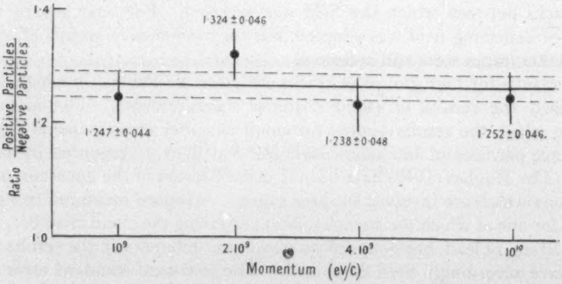

Figure 3. Ratio of positive and negative particles as a function of momentum. The full horizontal line represents the mean value over the whole spectrum, and the broken lines indicate the standard error of this value.

but it is relevant here that approximately 3% of these particles should be of opposite sign to that indicated by the recorded deflection: of the particles of mean momentum 10^{10} ev/c. tabulated as "positive", 97% are positive and 3% negative, and similarly for those tabulated as "negative". There is accordingly a correction to be applied which tends to increase the ratio of positive to negative particles in this group. In Table 2 (and also in the total of all measurements in Table 1) the uncorrected ratio is given in brackets, and is followed by the corrected value.

§4. NATURE OF PARTICLES

It is usually assumed that the ratio of positive to negative particles which we have measured is that of μ-mesons: it is possible to obtain some confirmation of this assumption for the preliminary results of experiments undertaken in this laboratory by Mr. M. G. Mylroi* to investigate the penetration of considerable thickness of lead by particles the momenta of which have been measured in the spectrograph.

In part of this work the passage through about 50 cm. lead of 3,500 particles, all of which were of sufficient momentum, if μ-mesons, to traverse the absorber, was examined. Of these particles 69 were not detected emerging from the absorber (either because the particles failed to penetrate or because of inefficiency of detection below the lead), 42 being positive and 27 negative.

We conclude that at least 98% of the particles used in our experiment are capable of penetrating about 50 cm. of lead, and these, in the present state of knowledge, must almost certainly be considered to be μ-mesons. The rather large positive excess in the small group of particles for which penetration was not observed by Mylroi would lead to a slight reduction of positive–negative ratio of the remaining particles, from $1{\cdot}268 \pm 0{\cdot}023$ to $1{\cdot}259 \pm 0{\cdot}024$; it will be noted that, since the effect is a small correction, the statistical weakness of the rejected group has little effect on the uncertainty of the main group.

A result differing from that given in Table 1 by not more than 1 or 2 per cent therefore applies to those particles capable of penetrating about 50 cm. of lead, which, as stated above, must almost certainly be considered to be μ-mesons.

§5. DISCUSSION

The agreement between our results and those of other workers using comparable methods shown in Table 1 requires no comment. Other results are, that at sea-level in the momentum range $10^9 - 10^{10}$ ev/c. there is no variation of the ratio of positive to negative particles to the statistical accuracy of our measurements, and that our experimental value of this ratio applies, to within 1 or 2%, to particles capable of traversing about 50 cm. of lead.

Agreement with results obtained by means of the magnetic focusing method of Bernardini and his co-workers (1941) is less satisfactory; for example, Quercia, Rispoli and Sciuti (1948) find a value 1·16 for the positive–negative ratio at sea-level (a notation differing from ours is used by these and other workers with this technique). The magnetic focusing method is essentially indirect, in that large corrections must be made to the observed quantities, and it therefore seems reasonable to attach more weight to the direct measurements which do not appear to be subject to any uncertainty from which the focusing method is free.

In a recent report, Ballario, Benini and Calamai (1948) describe measurements, using the magnetic focusing method, in which the positive–negative ratio is studied as a function of zenith angle. The ratio is found to decrease with increasing zenith angle and if, in each direction, the ratio is assumed to be independent of momentum, the zenith value of 1·16 is reduced to about 1·06 at 60°. This result is interpreted as demonstrating that the positive–negative ratio at meson formation depends closely upon energy; in particular the ratio is small for particles capable of reaching sea-level at an inclination of 60°, i.e. particles which must have been of energy greater than 4×10^9 ev. at formation, and the larger ratio found in the vertical direction is attributed to a large excess of positive particles in the energy range 2×10^9–4×10^9 ev. which can penetrate to sea-level vertically, but not at a zenith angle of 60°.

---

* We are indebted to Mr. Mylroi for making his data available to us.

Our measurements give no support to this conclusion. If we make the assumption that there is no significant differential absorption of fast mesons in the atmosphere, the results of Table 2 show no measurable variation of the positive–negative ratio over the energy range at formation, 3×10^9 ev. – 12×10^9 ev. Since the reduction in sensitivity at high momenta in the magnetic lens apparatus is likely to be considerable at momenta lower than the highest reached in our apparatus, these results include the whole group of particles for which Ballario and his co-workers deduce a very small excess of positive particles. The results of the zenith angle experiment must then be attributed either to differential absorption effects or to an uncertainty in the technique of measurement, as, for example, to the use of an incorrect form of momentum spectrum at large zenith angles.

§ 6. SIGNIFICANCE OF THE POSITIVE-NEGATIVE RATIO OF MESONS AND ITS MOMENTUM DEPENDENCE

In the absence of differential absorption of fast positive and negative mesons in the atmosphere, the ratio measured at sea-level must be directly connected to the ratio at formation. Further, the multiplicity of meson formation as a function of primary energy may be expected to determine the variation of positive–negative ratio at sea-level, although it is true that if meson formation is a plural process, or if the final states of the nucleons concerned are not equally probable, the relationship may be complicated.

Theoretical treatments which have been given (Heitler and Walsh 1945, Lewis, Oppenheimer and Wouthuysen 1948, Clementel and Puppi 1948) appear all to have discussed experimental values of the positive–negative ratio considerably smaller (∼1·15) than that which we now propose, and it is clearly of the greatest importance that this discrepancy should be resolved. It is interesting however that Jánossy and Nicolson (1947), using a simplified model—that a primary of energy E gives rise to N mesons each of energy E/N where N is constant—to investigate the geomagnetic effects, find that N must be of the order 9. While this result is largely dependent on observations with mesons of lower energy than those measured in our experiment, it is clear that this model would lead to a value close to our measurement and agreeing with it in so far as there is no measurable momentum variation of the ratio.

In a recent discussion of meson production, Lewis, Oppenheimer and Wouthuysen have derived a momentum dependence of the positive–negative ratio approximately of the form $\{(+/-)-1\}\sim\epsilon^{-\frac{1}{2}}$ where ϵ is the formation energy of the mesons. Our results at this stage do not completely exclude such a variation, which requires the quantity $\{(+/-)-1\}$ to vary by a factor two between the sea-level momenta 10^9 ev/c. and 10^{10} ev/c., but they do show it to be unlikely. More extensive data are now being collected which may be expected to establish more clearly the momentum dependence of the positive–negative ratio.

ACKNOWLEDGMENTS

The construction of the apparatus used in this investigation was made possible by a grant from the Treasury Fund of the Royal Society. The authors wish to thank Professor P. M. S. Blackett for his interest, encouragement and advice throughout the work, and are also grateful to Mr. M. G. Mylroi for his assistance in operating the spectrograph during the collection of data used in the investigation.

REFERENCES

Ballario, C., Benini, M., and Calamai, G., 1948, *Phys. Rev.*, **74**, 1729.
Bernardini, G., Conversi, M., Pancini, E., and Wick, G. C., 1941, *La Ric. Scient.*, **20**, 1227.
Blackett, P. M. S., 1937, *Proc. Roy. Soc.* A, **159**, 1.
Clementel, E., and Puppi, G., 1948, *Nuovo Cimento*, **5**, 529.
Heitler, W., and Walsh, P., 1945, *Rev. Mod. Phys.*, **17**, 252.
Hughes, D. J., 1940, *Phys. Rev.*, **57**, 592.
Jánossy, L., and Nicolson, P., 1947, *Proc. Roy. Soc.* A, **192**, 99.
Jones, H., 1939, *Rev. Mod. Phys.*, **11**, 235.
Lewis, H. W., Oppenheimer, J. R., and Wouthuysen, S. A., 1948, *Phys. Rev.*, **73**, 127.
Quercia, I. F., Rispoli, B., and Sciuti, S., 1948, *Phys. Rev.*, **74**, 1728.
Rossi, B., 1948, *Rev. Mod. Phys.*, **20**, 537.

The Effect of Holes in a Reacting Material on the Passage of Neutrons

By D. J BEHRENS
Theoretical Division, Atomic Energy Research Establishment, Harwell, Berks.

Communicated by K. Fuchs ; *MS. received* 31*st March* 1949

ABSTRACT. In this paper we discuss the increase in the migration length of neutrons in a reactor caused by the presence of holes in the reactor. It is shown how this effect can be evaluated in terms of a simple geometric function of the shape of the holes, and it is found that, in addition to a variation as the inverse overall density of the material in the reactor, the migration length also contains a term which depends upon the size and shape of each hole. When the hydraulic radius of the hole becomes comparable to the mean free path of neutrons in the reactor material, this last term becomes dominant, and it is therefore desirable that all holes should be kept as small as possible. Holes which are totally enclosed, or which contain a uni-directional infinity (cylinders) all give results of the same order of magnitude, but anything in the nature of a two-dimensional plane gash leads to a theoretically infinite increase in the migration length, and hence to a serious escape of spare neutrons.

We have considered the cases both of holes of regular shape and of the interstices between a random arrangement of regular-shaped solid bodies.

§1. INTRODUCTION

In order to cool a high power nuclear reactor, it is necessary to introduce into the reactor sufficient space for the passage of the coolant. In many cases the substances used as coolants are of such a low density that neutron scattering and absorption by the coolant does not occur to any appreciable extent, and, for the purposes of calculating the passage of neutrons through the reactor, we may treat the coolant spaces as though they were empty holes. Holes may also be required to provide space for experiments to be carried out in the reactor. If collisions between neutrons and the coolant can be disregarded, the reproductive constant *k* of the reactor [*] is unaffected by the presence of holes, and the number *N* of collisions made by the average neutron during its lifetime (or during any stage of its life, e.g. slowing down, or thermal diffusion) is also unchanged.

However, owing to the introduction of holes, the scattering atoms of the reactor are less closely spaced than they would be without holes. This effectively raises the mean free path of neutrons in the system, and the average direct distance "as the crow flies" covered in the course of *N* collisions increases in the same proportion.

If the holes are small and closely spaced, so that the mean free path in the solid material is large compared with the hole spacing, then the shape of the holes is of no consequence, and the effective mean free path varies inversely as the overall density of the reactor. Now the critical radius of a reactor of given shape varies as the effective mean free path, i.e. inversely as the density. It follows that the critical volume therefore varies as the inverse cube, and the critical mass as the inverse square, of the overall density of the reactor.

When the holes are large compared with the mean free path in the solid material, this simple treatment is no longer correct. While the arithmetic mean free path is the same, for given overall density, whether many paths are slightly lengthened by small holes or whether a few paths are greatly lengthened by large holes, the root-mean-square free path is substantially greater in the latter case than in the former. And, since the scattering processes are random and near-isotropic, it is with root-mean-square averages that we must be concerned. Consequently the larger the holes at given overall density, the greater will be the increase in the critical dimensions of the reactor.

We can make an estimate of the nature of this size effect. It may be expected that the increase in the square of the mean free path will, apart from the density factor, contain a term proportional to the proportion of neutron paths which pass through the holes and to the square of the amount by which these paths are lengthened.

Let ϕ be the volume ratio of the holes to the material of the reactor, and $v\phi$ the volume of each hole. Then we may imagine that there is a cell of material of volume v surrounding each hole, which may be assigned to that hole. Let s denote the surface area of a hole and let λ be the mean free path in the solid material. We assume that the total volume of the reactor is large compared with the volume v of a single cell, and that in every direction the dimensions of the reactor are large compared with λ.

Then the proportion of neutron paths which pass through a hole will be proportional to the ratio of a surface layer λ thick over the surface of the hole to the total volume of material in the cell associated with the hole. This ratio is $\lambda s/v$.

The amount by which each path is lengthened must be proportional to the dimensions of the hole, i.e. to $\phi v/s$. Hence the additional size-effect correction to the mean square free path must vary as $(\lambda s/v)(\phi v/s)^2$. Bearing in mind that r, the hydraulic radius of the hole, varies as $\phi v/s$, we may say that the size-effect correction to λ^2 must be proportional to $\phi\lambda r$. Dividing by λ^2, we get a proportionate increase factor which must vary as $\phi r/\lambda$.

---

[*] k is the number of neutrons of the second generation which are born in the reactor as the result of processes induced by one neutron of the first generation. $(k-1)/k$ is the proportion of neutrons which are superfluous to those required to maintain the reaction, and which can therefore be used for experimental purposes—in addition of course to replenishing the losses by leakage from the surface of the reactor.

This argument is developed in the present report with accuracy and in detail. The numerical coefficient of the term $\phi r/\lambda$ will be found to vary according to the shape of the hole. For a spherical hole the coefficient is 9/8, and for an infinite circular cylindrical hole it is 4/3.

§2. PASSAGE OF NEUTRONS IN A SYSTEM WITHOUT HOLES

When, at a later stage, we consider the effect of holes, we shall assume that the ratio of capture probability to scattering probability at the end of each free path is unaffected by the presence of holes*, and hence that the total number N of collisions made by each neutron during its lifetime is unchanged. We shall see that the root-mean-square total distance (as the crow flies) travelled by a neutron during the course of a given number n of collisions is increased owing to the presence of holes in a ratio which for large n is independent of the actual value of n. Consequently we may disregard the statistical variation which occurs in N, the total number of collisions made by a neutron, and calculate what is the mean square distance travelled in the course of N collisions, without specifying just what the value N actually is. If the scattering processes are random, then the probability of any particular length of free path must fall off exponentially as the length is increased. If λ is the arithmetic mean free path, then the probability of a free path having a length between z and $z+\delta z$ is given by the expression

$$\frac{1}{\lambda}\exp(-z/\lambda)\delta z. \qquad \ldots\ldots(1)$$

Denote by L_0^2 the mean square direct distance, as the crow flies, travelled by a neutron in the course of N collisions. If λ is unchanged throughout the period considered, we have

$$L_0^2=\int_0^\infty z^2\frac{N}{\lambda}\exp(-z/\lambda)\,dz=2N\lambda^2 \qquad \ldots\ldots(2)$$

for isotropic scattering. We have made here the tacit assumption that the system is large compared with λ, so that we can integrate without undue error over the full range to infinity of z.

If the conditions of scattering are not isotropic, we still have $L_0^2=Nl^2$, but l^2 (which may be described as the transport mean square free path) is no longer equal to $2\lambda^2$. The result,

$$L_0^2=Nl^2, \qquad \ldots\ldots(2a)$$

is a general formula, and the particular relation $l^2=2\lambda^2$ holds good for isotropic scattering.

§3. PASSAGE OF NEUTRONS IN A SYSTEM WITH HOLES

Let us assume now that the system is interspersed with holes, each of which may be taken to be associated with a surrounding cell of material, of volume v, in which the mean free path is still λ. Let ϕ be the volume ratio hole/material, so that $v\phi$ is the volume of each hole.

---

* This assumption will clearly be justified if the composition of the material of the reactor is of the same nature in all regions in the vicinity of the hole.

Consider now straight passages through the hole in any given direction, as specified by the value of a unit-vector Ω. Let X be the length of such a passage, and let $\psi(X, \Omega)\delta X$ denote the cross section of passages through the hole in the direction Ω which have lengths between X and $X+\delta X$.

Integrating, for any value of Ω, we must have

$$\int_0^\infty X\psi(X,\Omega)\,dX = \phi v. \qquad \ldots\ldots(3)$$

The integral is given as extending to infinity, although of course $\psi(X, \Omega)=0$ for all X in excess of the maximum diameter of the hole.

The quantity $\int_0^\infty \psi(X, \Omega)\,dX$ is in general a function of the direction Ω, as the hole has different projected areas in different directions, except in the special case where it is spherical. Now every passage cuts the surface of the hole twice, once on entering and once on leaving. It is clear that we can write

$$\int_0^\infty \psi(X, \Omega)\,dX = \iint_s \tfrac{1}{2}\,|\boldsymbol{\Omega}\,.\,\mathbf{ds}|,$$

where the right-hand expression denotes the positive value of the scalar product of $\boldsymbol{\Omega}$ and $\mathbf{ds}$, i.e. the element of area multiplied by the cosine of the acute angle between Ω and the normal to the surface.

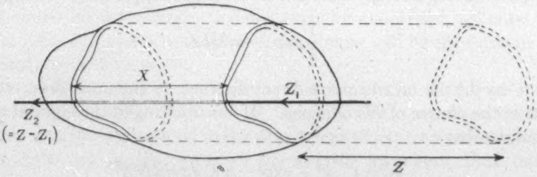

Cross section of annulus is $\psi(X, \Omega)\,\delta X$.

Averaging over all directions, we get

$$\int_\Omega \int_0^\infty \psi(X,\Omega)\,dX\,\frac{d\Omega}{4\pi} = \int_\Omega \iint_s \tfrac{1}{2}\,|\boldsymbol{\Omega}\,.\,\mathbf{ds}|\,\frac{d\Omega}{4\pi} = \tfrac{1}{4}s, \qquad \ldots\ldots(4)$$

since the mean value of the cosine is $\tfrac{1}{2}$.

Now let $p(z, \Omega, X)\delta X$ denote the probability that, during the course of a free path in the material of length z in the direction Ω, a neutron will emerge into a hole where the passage length lies between X and $X+\delta X$. Then it is clear that (see diagram)

$$p(z, \Omega, X) = z\psi(X, \Omega)/v. \qquad \ldots\ldots(5)$$

First of all we shall treat the holes as being widely separated, i.e. $v \gg s\lambda$, so that no neutron need ever be considered to pass through more than one hole in the course of a single free path. If ϕ is not very small, this implies the case of large holes.

The probability that a free path in the direction Ω will be increased in length from z to $z+X$, owing to the presence of a hole, is given by $p(z, \Omega, X)$.

Therefore we get, instead of (2) above, the equation

$$L^2 = N\int_\Omega \int_0^\infty \left[\int_0^\infty (z+X)^2 p(z,\Omega,X)\,dX + z^2\left\{1 - \int_0^\infty p(z,\Omega,X)\,dX\right\}\right]$$
$$\times \frac{1}{\lambda}\exp(-z/\lambda)\,dz\,\frac{d\Omega}{4\pi}$$
$$= 2N\lambda^2 + 4\phi N\lambda^2 + N\int_\Omega \int_0^\infty \frac{\lambda}{v} X^2 \psi(X,\Omega)\,dX\,\frac{d\Omega}{4\pi}, \qquad \ldots\ldots(6)$$

which may be combined with (2) to give

$$L^2/L_0^2 = 1 + 2\phi + \frac{1}{2\lambda v}\int_\Omega \int_0^\infty X^2 \psi(X,\Omega)\,dX\,\frac{d\Omega}{4\pi}. \qquad \ldots\ldots(7)$$

This is the general formula for the case of widely separated holes. If, instead of equation (2), we use the more general form (2 *a*), this results in the same proportionate change in L^2 as in L_0^2, and equation (7) therefore still holds good.

Consider now the opposite extreme, where the holes are very closely spaced, i.e. $v \ll s\lambda$. In the limit, the probability of entering a hole is independent of any holes which may already have been entered during the current free path.

The probability of entering no hole at all during a free path in the material of length z in the direction Ω is $\exp\left[-\int_0^\infty p(z,\Omega,X)\,dX\right]$, say $\exp[-P(z,\Omega)]$.

The probability of entering n holes, of lengths respectively $X_1, X_2 \ldots X_n$, can be shown to be

$$\frac{1}{n!}\prod_{j=1}^{n}[p(z,\Omega,X_j)]\exp[-P(z,\Omega)].$$

Hence we obtain, instead of the factor between the square brackets in (6) above, the corrected expression

$$\left[z^2\exp[-P(z,\Omega)] + \sum_{n=1}^{\infty}\left\{\prod_{j=1}^{n}\int_0^\infty\right\}\frac{\exp[-P(z,\Omega)]}{n!}\left(z + \sum_{j=1}^{n} X_j\right)^2\right.$$
$$\left.\times \prod_{j=1}^{n} p(z,\Omega,X_j)\prod_{j=1}^{n} dX_j\right]. \qquad \ldots\ldots(6\,a)$$

This expression can, without undue trouble, be separated into three parts, the coefficients respectively of the second, first and zero powers of z, and reduces to the form

$$z^2(1+\phi)^2 + \int_0^\infty X^2 p(z,\Omega,X)\,dX,$$

so that, instead of (7), we get the expression

$$L^2/L_0^2 = 1 + 2\phi + \phi^2 + \frac{1}{2\lambda v}\int_\Omega \int_0^\infty X^2 \psi(X,\Omega)\,dX\,\frac{d\Omega}{4\pi}. \qquad \ldots\ldots(8)$$

This differs from (7) in the addition of a ϕ^2 term.

When v and $s\lambda$ are of the same order, the average number of holes entered during the course of a free path of length Z in the solid is still $Zs/4v$. Suppose this number to be $(n+\epsilon)$, where n is an integer and ϵ a fraction between the limits

0 and 1. We shall examine the case in which it is assumed that, for a free path of length Z, there is a probability ϵ of entering $(n+1)$ holes, and $(1-\epsilon)$ of entering n.

Then if X is the lengthening per hole of the passage Z, we get, instead of Z^2 in equation (2), the quantity

$$\epsilon(Z+X_1+X_2+\ldots\ldots+X_{n+1})^2+(1-\epsilon)(Z+X_1+X_2+\ldots\ldots+X_n)^2.$$

Instead of the expression (6*a*) we therefore obtain

$$\begin{aligned}&\epsilon\left[\left(Z+\sum_{j=1}^{n+1}X_j\right)^2\prod_{j=1}^{n+1}\left\{\frac{p(z,\Omega,X_j)}{P(z,\Omega)}\right\}\prod_{j=1}^{n+1}dx_j\right]+(1-\epsilon)\left[\left(Z+\sum_{j=1}^{n}X_j\right)^2\right.\\&\qquad\qquad\left.\times\prod_{j=1}^{n}\left\{\frac{p(z,\Omega,X_j)}{P(z,\Omega)}\right\}\prod_{j=1}^{n}dX\right]\\&=\epsilon\left[Z^2+(n+1)2z\overline{X}+(n+1)\overline{X^2}+n(n+1)\overline{X}^2\right]\\&\qquad\qquad+(1-\epsilon)\left[Z^2+n2Z\overline{X}+n\overline{X^2}+n(n-1)\overline{X}^2\right]\\&=Z^2+2Z\overline{X}(n+\epsilon)+\overline{X^2}(n+\epsilon)+\overline{X}^2(2n\epsilon+n^2-n).\end{aligned}$$

Putting now $\overline{X}=4\phi v/s$, $\overline{X^2}=16Q\phi^2v^2/s^2$ and $Z=(n+\epsilon)4v/s$, we get the expression

$$Z^2+2Z^2\phi+4Qv\phi^2z/s+(16\phi^2v^2/s^2)(2n\epsilon+n^2-n).$$

The probability of occurrence of $(Z,\delta Z)$ is $(1/\lambda)\exp(-z/\lambda)\,dz$, so that the corresponding probability of $(n,\epsilon,\delta\epsilon)$ is $(4v/s\lambda)\exp[-(n+\epsilon)4v/s\lambda]\,d\epsilon$.

We have therefore to evaluate

$$\begin{aligned}&\int_0^\infty(z^2+2z^2\phi+4Qv\phi^2z/s)\frac{1}{\lambda}\exp(-z/\lambda)\,dz\\&\qquad\qquad+\int_{\epsilon=0}^{1}\sum_{n=0}^{\infty}\exp(-4vn/s\lambda)\frac{4v}{s\lambda}\,\frac{16\phi v^2}{s^2}(2n\epsilon+n^2-n)\,d\epsilon\\&\quad=2\lambda^2+4\lambda^2\phi+4Q\phi^2v\lambda/s+2\phi^2\lambda^2(4v/s\lambda)/[\exp(4v/s\lambda)-1]\end{aligned}$$

Dividing by $2\lambda^2$, we obtain the result that

$$L^2/L_0^2=1+2\phi+\phi^2(4v/s\lambda)/[\exp(4v/s\lambda)-1]+\frac{1}{2\lambda v}\int_\Omega\int_0^\infty X^2\psi(X,\Omega)\,dX\frac{d\Omega}{4\pi}. \qquad \ldots\ldots(9)$$

It may be verified that, if $v\gg s\lambda$, equation (9) reduces to (7), while if $v\ll s\lambda$ it gives the same result as (8). The last expression is therefore a form which may reasonably be used to cover holes of all sizes.

Now in the case of coolant channels it is customary to define a hydraulic radius, which is given by $r=2\phi v/s$ (so that, for an infinite circular cylinder, r is in fact the radius of the cylinder). It is convenient to use this notation for all holes, so that we may re-write (9) in the form

$$L^2/L_0^2=1+2\phi+\phi^2(2r/\phi\lambda)/[\exp(2r/\phi\lambda)-1]+Qr\phi/\lambda, \qquad \ldots\ldots(10)$$

where

$$Q=(1/r^2s)\int_\Omega\int_0^\infty X^2\phi(X,\Omega)\,dX\frac{d\Omega}{4\pi}. \qquad \ldots\ldots(11)$$

(10) is a general expression for holes of any kind, while (11) shows Q to be a function only of the shape of the hole. Q is the mean square passage length through the hole divided by the square of the mean, and hence must exceed unity.

Values of Q for particular shapes of hole are as follows:

Spherical hole	$Q=1{\cdot}125$
Regular tetrahedron hole	$Q=1{\cdot}583$
Infinite cylinder of circular section	$Q=1{\cdot}333$
Infinite cylinder of regular hexagonal section	$Q=1{\cdot}397$
Infinite cylinder of square section	$Q=1{\cdot}487$
Infinite cylinder of equilateral triangular section	$Q=1{\cdot}648$
Cored spherical hole	$Q=1{\cdot}125\times f(\mu)$
Cored circular cylinder	$Q=1{\cdot}333\times F(\mu)$

(where μ = inner-radius/outer-radius, and f and F are tabulated below).

μ	0·0	0·1	0·2	0·3	0·4	0·5	0·6	0·7	0·8	0·9	1·0
$f(\mu)$	1·000	1·001	1·005	1·016	1·04	1·07	1·11	1·18	1·27	1·43	∞
$F(\mu)$	1·0000	1·0258	1·0536	1·0839	1·1178	1·1567	1·2023	1·2604	1·3422	1·53	∞

The fact that f and F tend to infinity as $\mu\to 1$ is in accord with the result that Q is infinite for a two-dimensionally infinite gash extending through the reactor.

The term in ϕ^2 falls away rapidly as $r/\lambda\phi$ increases. When r reaches the value $3\tfrac{1}{4}\lambda\phi$, this term is already less than $\phi^2/100$. The final term in (10) however increases more rapidly than the other decreases, as may be shown by re-writing (10) in the form

$$L^2/L_0^2=1+2\phi+(r\phi/\lambda)[\coth(r/\phi\lambda)+(Q-1)]. \qquad \ldots\ldots(12)$$

Since, as we have seen, Q cannot be less than unity, $Q-1$ is essentially non-negative. Again, $\coth(r/\phi\lambda)$ is at least as great as $\phi\lambda/r$, its limiting value as $r/\phi\lambda\to 0$. Thus L^2/L_0^2 is in all cases at least as great as $(1+\phi)^2$.

The following typical values of L^2/L_0^2 apply to a square lattice of cylindrical holes:

Lattice spacing / Hole diameter	10	5	3	2
r/λ very small	1·016 *1·000*	1·066 *1·000*	1·200 *1·000*	1·548 *1·000*
$r/\lambda=\frac{1}{3}$	1·019 *1·003*	1·079 *1·012*	1·234 *1·028*	1·609 *1·039*
$r/\lambda=1$	1·026 *1·010*	1·108 *1·039*	1·319 *1·099*	1·815 *1·172*
$r/\lambda=3$	1·047 *1·031*	1·194 *1·066*	1·574 *1·312*	2·466 *1·593*

In each case the upper figure is the value of L^2/L_0^2 obtained by the use of (12). The lower figure in italics is the ratio of this value to the simple density correction $(1+\phi)^2$.

§4. ANISOTROPIC EFFECTS

In all cases except those of spherical holes (with or without concentric cores) we have seen that $\int_0^\infty \psi(X,\Omega)\,dX$ and $\int_0^\infty X^2\psi(X,\Omega)\,dX$ vary with Ω.

This means that L^2, instead of having a component $L^2/3$ in all directions, becomes an anisotropic function.

Examining equation (10), and the argument by which we established the equation, it is clear that only the function Q contributes an anisotropic term to L^2, and that the contribution in any direction is given by

$$\int_\Omega (1/2\lambda v) \int_0^\infty X^2 \cos^2 w \psi(X, \Omega)\, dX \frac{d\Omega}{4\pi},$$

where w is the angle between the direction under consideration and the direction of Ω.

For all cylindrical holes (plain or cored, and of any section) we get an effect twice as great in the axial as in the transverse directions:

$$\left.\begin{aligned} 3L^2_{\text{axial}}/L_0^2 &= 1 + 2\phi + \phi^2(2r/\phi\lambda)/[\exp(2r/\phi\lambda) - 1] + \tfrac{3}{2} Qr\phi/\lambda, \\ 3L^2_{\text{transv.}}/L_0^2 &= 1 + 2\phi + \phi^2(2r/\phi\lambda)/[\exp(2r/\phi\lambda) - 1] + \tfrac{3}{4} Qr\phi/\lambda, \end{aligned}\right\}$$

where Q is still the average value for all directions, namely 1·333 for a circular cylinder, 1·487 for one of square section, etc. It may be verified that ΣQ for the three directions at right angles is unchanged, for $\frac{3}{2} + 2(\frac{3}{4}) = 3$.

§5. HOLES FORMED AS INTERSTICES BETWEEN A RANDOM ARRANGEMENT OF SOLID BODIES IN POINT OR LINE CONTACT

Hitherto we have dealt only with the case of holes of a regular shape. Sometimes however we are concerned with the holes which arise as interstices between a random arrangement of solid bodies. We shall assume that the solid bodies are in point or line contact, but nowhere in surface contact, so that the total surface area of the bodies will be equal to that of the holes.

Let $\overline{X}$ and $\overline{X'}$ denote respectively the mean passsage length through a hole and through a solid body respectively. Then, if V is the total volume of a large part of the reactor, and S is the surface area of hole (or solid) within V, we have

$$\overline{X} = \frac{\phi}{1+\phi} \frac{4V}{S}; \qquad \overline{X'} = \frac{1}{1+\phi} \frac{4V}{S}.$$

Also, by the definition of Q,

$$\overline{X^2} = \frac{\phi^2}{(1+\phi)^2} Q \frac{16V^2}{S^2}$$

and, defining Q' by analogy,

$$\overline{X'^2} = \frac{1}{(1+\phi)^2} Q' \frac{16V^2}{S^2}.$$

Now, if the bodies are randomly arranged, there will be no correlation between the values of X and of $(X + X')$ measured in one and the same straight line. Consequently we have not only $\overline{X} = (4V/S) - \overline{X'}$, but also

$$\overline{X^2} = \frac{16V^2}{S^2} - \frac{8V}{S} \overline{X'} + \overline{X'^2}. \qquad \ldots\ldots(13)$$

This result is equivalent to assuming that the mean square deviations of X and X' are equal, i.e. $\overline{X'^2} - \overline{X'}^2 = \overline{X^2} - \overline{X}^2$. For since $\overline{X} = (4V/S) - \overline{X'}$ we must have

$$\overline{X}^2 = \frac{16V^2}{S^2} - \frac{8V}{S} \overline{X'} + \overline{X'}^2$$

and if $\overline{X^2} - \overline{X}^2 = \overline{X'^2} - \overline{X'}^2$.

Then, adding, we obtain equation (13) which, from the equations above, gives

$$\frac{\phi^2}{(1+\phi)^2}Q\frac{16V^2}{S^2}=\frac{16V^2}{S^2}-2\frac{1}{1+\phi}\frac{16V^2}{S^2}+\frac{1}{(1+\phi)^2}Q'\frac{16V^2}{S^2}.$$

Multiplying by $(1+\phi)^2$ and dividing by $16V^2/S^2$, we get

$$\phi^2Q=(1+2\phi+\phi^2)-(2+2\phi)+Q', \quad \text{i.e.} \quad (Q-1)=(Q'-1)/\phi^2. \quad \ldots\ldots(14)$$

Likewise, if r denotes the hydraulic radius of the hole and r' that of the solid, we have

$$r=2V_{\text{hole}}/S_{\text{hole}}, \qquad r'=2V_{\text{solid}}/S_{\text{solid}}.$$

But the S's are equal, so that $r=r'V_{\text{hole}}/V_{\text{solid}}$, or

$$r=r'\phi. \quad \ldots\ldots(15)$$

Substituting in (12) from (14) and (15) we get

$$L^2/L_0^2=1+2\phi+\frac{r'}{\lambda}\left(\phi^2\coth\frac{r'}{\lambda}+(Q'-1)\right). \quad \ldots\ldots(16)$$

Thus we can calculate the streaming effect not only for regular holes but also for those formed between a random arrangement of regular solids. In such cases ϕ is often large, and the coth term must be taken into account. Algebraically, also, equation (12) containing $Q-1$ is more suitable for substitution by (14) than is (10), which contains Q itself.

§ 6. CONCLUSIONS

The migration length M of neutrons in a system is defined so that $6M^2$ is the mean square distance travelled by a neutron in the whole course of its life. This includes the time spent whilst the neutron is slowing down from its initial energy and the time spent whilst diffusing as a thermal neutron until it is finally absorbed.

The critical size of a reactor depends on $M^2/(k-1)$, and, therefore, the migration length is an important design quantity. For a given size of reactor we shall be interested in keeping the migration length as small as possible, since a decrease in M^2 means that a lower value of k is required to maintain the reaction. Now the value of k required to maintain the reaction is less than that produced by the lattice by a quantity Δk, usually referred to as "spare k", which (while taken up by control rods when not otherwise being utilized) may provide an excess of neutrons for experimental purposes, e.g. irradiation of materials for isotope production.

The theory developed in this paper may be applied to any stage of the neutron's history, provided of course the statistical methods employed are applicable, i.e. within the scope of the age velocity theory and the simple neutron diffusion theory. It is clear that the values of L^2/L_0^2 which we have calculated can be applied directly to the migration length, to give M^2/M_0^2, where M_0 is the migration length in a system without holes.

To summarize: the effect of holes on M^2 is made up of two parts: firstly, there is an isotropic increase in M^2 proportional to $(1+\phi)^2$, i.e. the inverse square of the overall density of the material. In addition to this, there is a further correction term, proportional to the ratio of the hydraulic ratio of the hole to the mean free path in the solid, the volume ratio ϕ, and to a function Q of the shape of the hole. Q is in fact the ratio of the mean square chord length through the hole to the square of the mean chord length, and is least for a sphere (for which it is 9/8). For totally enclosed and cylindrical holes, Q varies between fairly narrow limits, being seldom in excess of 5/3 for reasonable shapes. Any more than unidirectional infinity, however, by offering very long chords over a finite solid angle, results in a theoretically infinite increase of Q, and, even in the case of a finite reactor surrounded by a reflector, to a substantial increase in M^2, and hence to a serious loss of spare k. Such multi-directional holes (e.g. plane gashes) are therefore, if possible, to be avoided from the point of view of conservation of neutrons within the system.

NOTATION

k = reproductive constant of reactor.
N = number of collisions made by a neutron.
λ = mean free path of a neutron through solid material of reactor.
l^2 = transport mean square free path (for isotropic scattering, $l^2 = 2\lambda^2$).
ϕ = volume ratio: holes/material.
$v\phi$ = volume of each hole.
s = surface area of each hole.
S = surface area of a cell.
V = volume of a cell.
r = hydraulic radius of each hole: $r = 2v\phi/s$.
z = length of a (specified) free path through solid material.
L_0 = root-mean-square distance travelled by a neutron in N collisions in the absence of holes.
L = root-mean-square distance travelled by a neutron in N collisions in the presence of holes.
X = length of a straight passage through a hole.
$\mathbf{\Omega}$ = unit vector specifying direction.
$\psi(X, \Omega)\,\delta X$ = cross section of passages of length between X and $X+\delta X$ in the direction $\mathbf{\Omega}$ through a hole.
$p(z, \Omega, X)$ = probability that a neutron, during the course of a free path of length z in the direction $\mathbf{\Omega}$, will emerge into a passage of length X.
$P(z, \Omega) = \int_0^\infty p(z, \Omega, X)\,dX$.
Q = ratio of mean square passage length through hole to square of mean passage length, so that we have

$$Q = \frac{1}{r^2 s}\int_\Omega \int_0^\infty X^2 \psi(X, \Omega)\,dX\,\frac{d\Omega}{4\pi}.$$

μ = ratio of inner to outer radius for a cored hole.
M = migration length of neutrons.

Betatron Injection into Synchrotrons

By F. K. GOWARD
Atomic Energy Research Establishment, Harwell, Didcot, Berks.

Communicated by D. Taylor ; MS. received 13th December 1948, and in amended form 23rd May 1949

ABSTRACT. The paper states simply the factors influencing the proportion of electrons which may be trapped and accelerated in a transition from betatron to synchrotron operation; this transition is a vital factor influencing the design of the normal electron-synchrotron. Machines of various energies are studied, and it is shown that the important considerations in the design are quite different in different energy ranges. The theoretical predictions are compared with experimental evidence obtained on 14 and 70 MeV. synchrotrons, and the agreement is sufficient to give confidence in the simplified theory.

§1. INTRODUCTION

SEVERAL adequate papers on the theory of electron-synchrotron operation have been published; it will be convenient to choose only one of them (Bohm and Foldy 1946) as the theoretical basis of the discussion which follows and to assume the results given there without further proof. These theoretical papers have given little detailed attention to the experimental behaviour to be expected from machines of various energies. Such consideration is very necessary, since electron-synchrotrons are now being operated or constructed in Britain (and elsewhere) with energies ranging from 14 to 375 MeV., and factors of importance at one energy are quite unimportant at other energies.

To emphasize the difference between the various machines, an idealized picture will be presented of the fraction of electrons captured during the transition from betatron to synchrotron. The process will be over-simplified to separate clearly the more important physical effects, and experimental evidence will be advanced to justify the simplification made. Such a simplified theory is very desirable for general comparison between machines (see for example the paper on synchrotron resonator design by Goward *et al.* 1949) and for initial design purposes. The more exact theories may be applied for more particular considerations.

§2. THEORY OF INJECTION

2.1. *General Factors Influencing Injection Efficiency*

The minimum resonator voltage, v, required to accelerate an electron, if it happens to be at precisely the optimum phase and radius when it is injected from the betatron to the synchrotron, is given by

$$v = 4\pi^2 \mathbf{c}^{-1} f E r_0 \cos 2\pi f t, \qquad \ldots\ldots(1)$$

where f is the frequency of the magnetic field in cycles/sec., E is the peak energy of the machine in electron volts, and r_0 is the equilibrium orbit radius in centimetres. v is maximum at the start of the acceleration, and since r_0 is increased proportionately to E for the various synchrotrons, v_0, the maximum value of v is proportional to E^2. Taking a peak field of 10,000 gauss, r_0 is equal to $10^{-6}E/3$, and, therefore, if f is 50,

$$v_0 = 2{\cdot}2 \times 10^{-14} E^2. \qquad \ldots\ldots(2)$$

Electrons are normally injected into a synchrotron not only at the correct phase and radius but over quite a range of radii and phases. The resonator voltage must, therefore, be somewhat greater than v_0, how much greater depending in a rather complex manner on the size of the machine and its operating parameters.

If the electrons are accelerated by betatron action from an initial total energy, E_{I}, to a final total energy, E_s, and the betatron action then ceases suddenly, an electron beam is obtained with a spread of radii given by

$$\rho_0 = \rho_{\mathrm{I}}(E_{\mathrm{I}}\beta_{\mathrm{I}}/E_s\beta_s), \qquad \ldots\ldots(3)$$

where β is the velocity of the electrons relative to the velocity of light. The spread of radii, $\pm\rho_{\mathrm{I}}$, about the equilibrium orbit radius r_0, is, for the moment, assumed to fill the donut entirely at injection, and the energy of the electrons is assumed to be that corresponding to an instantaneous circle at their particular radii, i.e. oscillations about the instantaneous circle are neglected. It is also assumed that the electrons are distributed uniformly in phase and in radius between the limits $r_0 - \rho_0$ and $r_0 + \rho_0$.

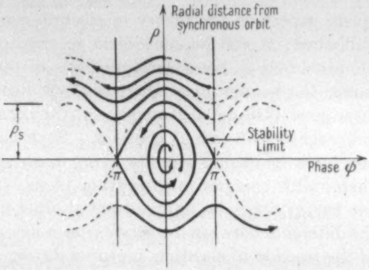

Figure 1. Oscillations in phase and radius ($V \gg v_0$).

Suppose, now, that the betatron action ceases suddenly and that a voltage V is supplied suddenly to the R.F. resonator, the frequency being such that the synchronous orbit coincides with the betatron equilibrium orbit. The resonator may be considered as producing a wave which travels round the synchrotron with the same angular velocity as the electrons injected from the betatron. Provided the voltage V is considerably greater than v_0 the electrons will tend to oscillate approximately sinusoidally in phase about the zero phase point. This follows from the relation giving the phase, ϕ_s, at which the electrons are accelerated without oscillations, which is

$$\sin\phi_s = v_0/V. \qquad \ldots\ldots(4)$$

To the phase oscillations correspond equivalent oscillations in radius or energy. These oscillations are represented in Figure 1, where the phase is measured relative to the R.F. wave. It may be seen that, if the spread of radii of the electrons before the radio frequency is turned on is $\pm\rho_0$, the final spread of those electrons which are caught is $\pm\rho_s$, where ρ_s is marked on the figure. Only those electrons are trapped which lie within the curve marked "stability limit"; electrons outside this region lose or gain phase continuously as shown. It is assumed that electrons are caught provided

$$\rho < \rho_s \cos\phi/2. \qquad \ldots\ldots(5)$$

ρ_s is given by Bohm and Foldy as

$$\rho_s = \frac{r_0}{(1-n)\beta_s^2}\left[\frac{2V}{\pi k E_s}\right]^{\frac{1}{2}}, \qquad \ldots\ldots(6)$$

k being given by

$$k = 1 + \frac{n}{(1-n)\beta_s^2}, \qquad \ldots\ldots(7)$$

where n is the usual index in the magnetic field law. It may be seen that ρ_s/ρ_0 must be substantially greater than unity in order that a large proportion of electrons may be trapped. Examples of inefficient and efficient trapping are shown in Figures 2(*a*) and 2(*b*), where it is assumed that the resonator voltage, V, is varied to vary ρ_s, always keeping it very much greater than v_0. Figure 2(*c*) indicates what may happen if ρ_s is made so large that it exceeds the donut half-width, ρ_1. Electrons are then lost, even though they are trapped in stable oscillations. In the figure the period of rotation on the phase diagram of all electrons has been assumed constant; in fact the period decreases as the distance from the centre increases, so that A′B′ should be an S-shaped curve. This does not affect the fraction of electrons collected.

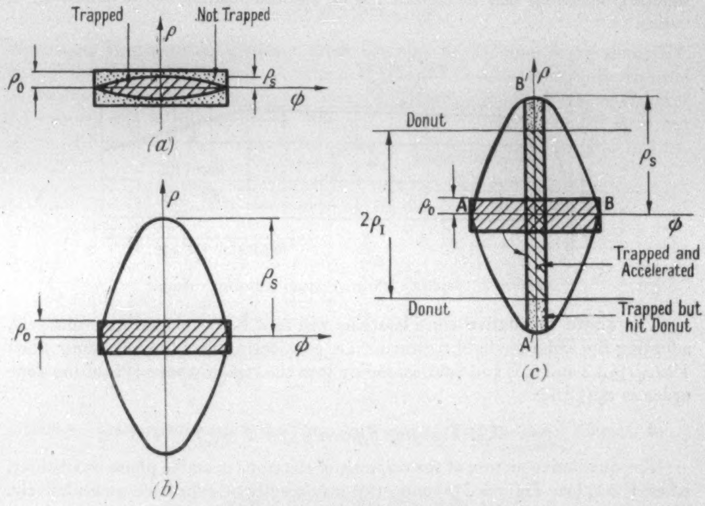

Figure 2. Trapping efficiency ($V \gg v_0$).

(*a*) Inefficient trapping (resonator volts small).
(*b*) Efficient trapping (resonator volts large).
(*c*) Efficient trapping but donut walls hit.

Qualitatively, then, the basic curve giving the fraction of electrons accelerated (i.e. injection efficiency) against resonator voltage may be expected to be of the form shown by the full curve in Figure 3, provided always that the voltage across the resonator, V, is substantially greater than the minimum voltage v_0 required to accelerate the electrons. It will be seen in §§ 2.2 and 2.3 that, not only is this basic curve of the same form for synchrotrons of various energies, but the absolute values of the resonator voltages at which the effects occur remain approximately constant.

The factor which does differ markedly in synchrotrons of different energies is the voltage v_0 defined by equation (2); this voltage is a few volts in the smaller energy machines and a few kilovolts in the larger energy machines. The efficiency does not rise suddenly to the full curve of Figure 3 at the voltage v_0, however, since the condition that V/v_0 is much greater than unity does not hold in this region and ϕ_s is therefore not zero (see equation (4)). Electrons are trapped over a limited range of phases only, and the efficiency rises to the curve of Figure 3 relatively gradually, as is shown qualitatively by the dotted curve. Widely differing behaviour may be expected as v_0, and the position of the dotted curve, varies.

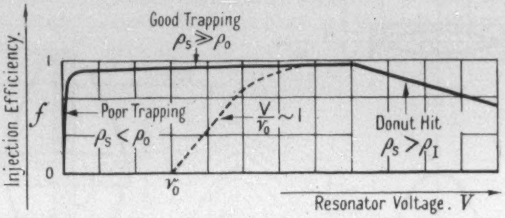

Figure 3. Injection efficiency versus resonator voltage.

The above qualitative considerations will now be developed quantitatively, adopting the same mode of treatment, i.e. considering first the behaviour when $V \gg v_0$ (§§ 2.2 and 2.3) and later extending it to the region where V is of the same order as v_0 (§ 2.4).

2.2. *Trapping Efficiency (for $V \gg v_0$)*

The qualitative picture of the trapping of electrons in stable phase oscillations, when $V \gg v_0$ (see Figures 2(*a*) and 2(*b*)) may readily be expressed quantitatively. Using the condition of equation (5), a simple integration shows that, for $\rho_0 \leqslant \rho_s$, the fraction of electrons trapped, f_1, is given by

$$f_1 = 1 - (2/\pi)[\sin^{-1}(\rho_0/\rho_s) - (\rho_s/\rho_0)\{1 - \cos\sin^{-1}(\rho_0/\rho_s)\}]. \quad \ldots\ldots(8)$$

For $\rho_0 \geqslant \rho_s$,

$$f_1 = 2\rho_s/\rho_0\pi. \quad \ldots\ldots(9)$$

Using equations (3) and (6), equations (8) and (9) may be expressed in terms of the parameter V/V_0 by the relation

$$(\rho_s/\rho_0) = (V/V_0)^{\frac{1}{2}}, \quad \ldots\ldots(10)$$

where

$$V_0 = \left[(1-n)^2 \beta_s^2 E_I^2 \beta_I^2 \left(\frac{\pi k}{2E_s}\right)\right]\left(\frac{\rho_I}{r_0}\right)^2. \quad \ldots\ldots(11)$$

The resulting curve for the fraction, f_1, plotted against V/V_0, is shown in Figure 4. The condition for loss of 36% or less of the electrons is

$$V \geqslant V_0. \quad \ldots\ldots(12)$$

Equation (12) gives a simple physical meaning to the parameter V_0 but V_0 is really a parameter derived from the constants of the machine by equation (11).

From equations (11) and (12) follows the interesting fact that the absolute minimum voltage required across the resonator for efficient trapping is practically invariant for different energy machines. This follows because electrons are normally injected into the betatron at the highest energy the standard type of gun permits, which makes E_I and β_I constant, and also because, for economy in iron and space, the change-over from betatron to synchrotron action is allowed to take place at as low an energy as possible, which gives $E_s = \text{constant}$. If the electrons are injected into the betatron at 50 kv., and the change-over to synchrotron operation occurs at $E_s = 2{\cdot}5$ MeV., equation (11) gives, for $n = 0{\cdot}7$,

$$V_0 = 0{\cdot}97 \times 10^4 (\rho_I/r_0)^2. \qquad \ldots\ldots(13)$$

Since ρ_I/r_0 is practically constant from machine to machine, being about 1/8, V_0 is of the order of 150 volts. A voltage of at least 150 volts is therefore required on the resonator of a synchrotron to obtain efficient trapping. This condition is a necessary one in all conditions, but may not be a sufficient one if v_0 is not appreciably less than V_0. This latter condition will be discussed in detail in § 2.4.

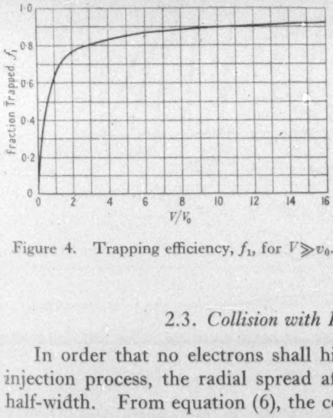

Figure 4. Trapping efficiency, f_1, for $V \gg v_0$.

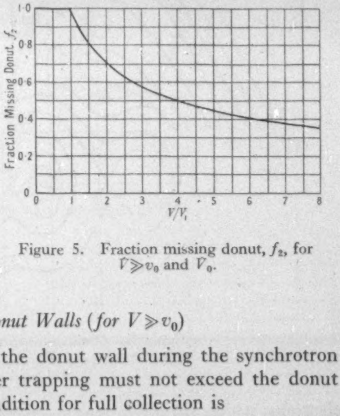

Figure 5. Fraction missing donut, f_2, for $V \gg v_0$ and V_0.

2.3. *Collision with Donut Walls (for $V \gg v_0$)*

In order that no electrons shall hit the donut wall during the synchrotron injection process, the radial spread after trapping must not exceed the donut half-width. From equation (6), the condition for full collection is

$$V \leqslant V_1, \qquad \ldots\ldots(14)$$

where

$$V_1 = [\tfrac{1}{2}(1-n)^2 \beta_s^4 \pi k E_s](\rho_I/r_0)^2. \qquad \ldots\ldots(15)$$

Equation (14) gives a simple physical meaning to the parameter V_1, but V_1 is (cf. V_0) really a parameter derived from the constants of the machine by equation (15). Substituting the same values as for equation (13) we obtain the result

$$V_1 = 1{\cdot}11 \times 10^6 (\rho_I/r_0)^2 = 17\,\text{kv}. \qquad \ldots\ldots(16)$$

V_1 is not only approximately constant from machine to machine, as V_0 is, but it is also independent of voltage of injection into the betatron.

If V is greater than V_1, then, since ρ_s is proportional to $V^{\frac{1}{2}}$ by equation (6), the fraction of those electrons trapped which escape collision with the donut is given by

$$f_2=(V_1/V)^{\frac{1}{2}}. \qquad \ldots\ldots(17)^*$$

This relation is readily deduced from Figure 2 (*c*), where it should be noted that a rotating line on the phase diagram is assumed, rather than a rotating area, as in Figure 2 (*a*), i.e. it is assumed not only that $V \gg v_0$, but also that $V \gg V_0$. The latter will always be so, since $V_1 \sim 100\ V_0$. The fraction f_2 is plotted in Figure 5.

It is interesting to observe that the condition for overlap of the rising and falling curves described by f_1 and f_2 is that $V_1 = V_0$, i.e. that $E_s = E_I$, or that the electrons should be injected directly into the synchrotron, without intermediary betatron acceleration.

2.4. *Corrections with* $V \sim v_0$

The discussion of §§2.2 and 2.3 is considerably modified if $V \sim v_0$. The electrons now oscillate about a phase ϕ_s given by equation (4). The range of phases and radii over which stable oscillations are possible is correspondingly reduced. The oscillations of Figure 1 are now replaced by oscillations such as those shown in Figure 6. This figure shows clearly the mechanism whereby electrons, which are at too large an energy and radius to be trapped, pass inwards to hit the donut wall; they pass through the synchronous radius via one of the gaps between the stable regions. The way in which the size of the stable region varies with V/v_0 is given by Bohm and Foldy. A figure similar to theirs, with the addition of a convenient scale of V/V_0, is shown in Figure 7. The fraction of electrons trapped for any value of V/v_0 and V/V_0 may be found directly by taking area ratios such as EFGH/ABCD on the figure. This fraction would correspond, in the example shown, to $V/V_0 = 16$ and $V/v_0 = 2$.

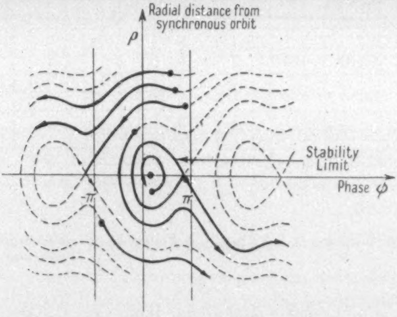

Figure 6. Oscillations in phase and radius for $V \sim v_0$. Note: The figure is to scale and shows the case where $V = 2v_0$, i.e. $\phi_s = 30°$.

Rather than consider the problem directly, as above, it is more instructive to consider various limiting conditions. Thus if V/V_0 is less than unity, the fraction trapped is merely f_1 multiplied by a fraction f_3; f_3 is the area of a curve such as EFL, corresponding to a particular V/v_0, relative to the area of the curve ABM, for which $V/v_0 = \infty$. This relationship is valid also for V/V_0 somewhat greater than unity, it being only necessary that the ordinate V/V_0 shall be greater than the maximum height of the particular V/v_0 curve. Thus for V less than, or of the order of, V_0, $(V/V_0 \lesssim 1)$, the fraction of electrons trapped is obtained by multiplying the fraction f_1 by the fraction f_3, shown in curve (a) of Figure 8.

---

* Equation (17) assumes a uniform distribution of electrons along A′B′ in Figure 2 (*c*). J. J. Wilkins has pointed out that a better approximation would be to assume a uniform distribution along AB, which gives $f_2 = (2/\pi) \sin^{-1}(V_1/V)^{\frac{1}{2}}$.

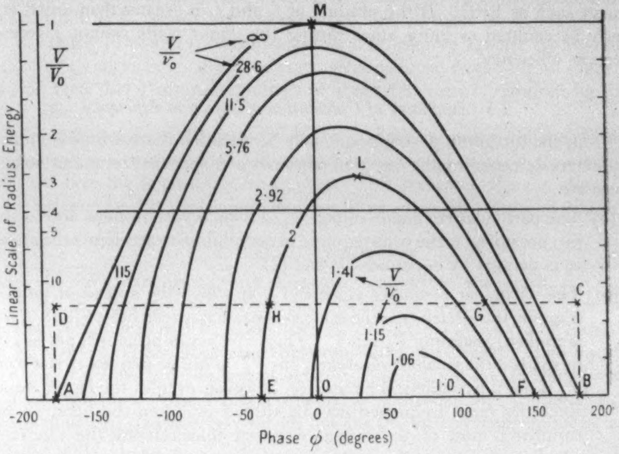

Figure 7. Stability limits for various values of V/v_0.

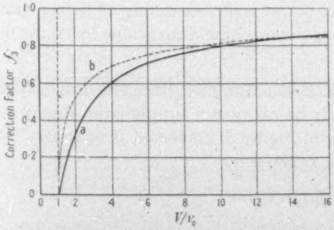

Figure 8. Correction, f_3, to f_1 when $V/v_0 \sim 1$.
Curve a: Approximation when $V/V_0 \lesssim 1$
Curve b: Approximation when $V/V_0 \gg 1$.

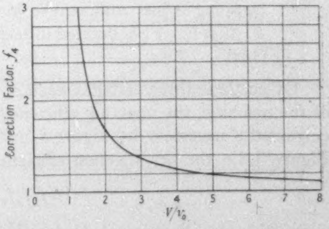

Figure 9. Correction, f_4, to f_2 when $V/v_0 \sim 1$.
$(V/V_0 \gg 1)$.

If V/V_0 is very much greater than unity, f_3 approaches the ratio of intercepts of the curves on the ϕ axis in Figure 7, e.g. $f_3 = \mathrm{EF}/\mathrm{AB}$. This ratio is shown in curve (b) of Figure 8.

To obtain the fraction trapped in the transition region between the two curves (a) and (b), the problem must be treated directly by the method already indicated.

It should be noted, however, that the transition curve does not, of necessity, lie between the two limiting curves, although, as will be seen in the examples to be studied, it does so very nearly.

The decrease in trapping efficiency in the region $V/v_0 \sim 1$ is compensated in certain circumstances by a decreased chance of hitting the donut walls, since there is only a small radial spread for the stable phase oscillations when $V/v_0 \sim 1$. To allow for this effect, f_2 in Figure 4 must be multiplied by a factor f_4 (see Figure 9). f_4 is the ratio of the height OM in Figure 7 to the maximum height of a curve such as EFL. If the product of f_2 and f_4 is greater than unity, it must clearly be counted as unity, since hitting the donut walls cannot increase the injection efficiency.

2.5. *Summary of Calculation of Injection Efficiency*

From the foregoing description it may be seen that there are three important parameters determining the injection efficiency at a specified resonator voltage V. These are

(*a*) The particular resonator voltage, v_0, at which synchronous acceleration is just possible, i.e. the volts required per revolution to accelerate the electrons. v_0 is defined by equations (1) and (2).

(*b*) The particular resonator voltage, V_0, at which the spread of radii, after trapping the electrons, is the same as the radial spread before the R.F. voltage is applied, assuming $V_0/v_0 \gg 1$. This latter assumption will not be correct in any but the smallest machines, but V_0 should be defined as if it were so. V_0 is not a hypothetical parameter, however, even in the larger machines since the radio frequency may be turned on when the betatron is still supplying most of the voltage required to accelerate the electrons, in which case v_0 is much smaller than the nominal value. V_0 is defined in terms of the machine dimensions by equation (11).

(*c*) The particular resonator voltage, V_1, at which the spread of radii after trapping it just sufficient to hit the donut walls, assuming as before that $V_1/v_0 \gg 1$. V_1 is defined in terms of the machine dimensions by equation (15).

Given these three voltages, each of which is determined from the dimensions of the machine, the injection efficiency may be calculated simply from Figure 4, corrected if necessary by Figure 8, and from Figure 5, corrected if necessary by Figure 9, i.e. the net injection efficiency f, is given by

$$f = f_1 f_2 f_3 f_4, \text{ if } f_2 f_4 < 1,$$
$$f = f_1 f_3, \text{ if } f_2 f_4 \geqslant 1. \qquad \ldots\ldots(18)$$

In circumstances where it is doubtful whether curve (a) or (b) of Figure 8 is appropriate, the efficiency should be obtained directly from Figure 7, by the method outlined in the opening paragraph of § 2.4. Calculation by equation (18) is by far the most convenient method, however, and should be used whenever possible.

The procedure described will now be illustrated by examples of machines operating at different energies. The specifications of the machines given will be nominal ones, since they are in early stages of development, where changes of specification are still permissible.

§ 3. EXAMPLES

3.1. 30 MEV. *Synchrotron*

The 30 MeV. synchrotron built by Fry *et al.* (1948) has $\rho_I = 1{\cdot}5$ cm., $r_0 = 10$ cm., $E_s = 2{\cdot}5$ MeV., 25 kv. injection voltage, and operates at 50 c/s. The basic parameters are therefore: $V/v_0 = 5{\cdot}4$; $v_0 = 20$ v.; $V_0 = 108$ v.; $V_1 = 25$kv. The high value of V_1 means that there is no possibility of hitting the donut wall during injection with any resonator voltage likely to be used. The injection efficiency, f, is therefore obtained by multiplication of f_1 and f_3. f_1 is the predominant factor and the $V \lesssim V_0$ approximation (curve (a)), may be taken for f_3. The dotted curve of Figure 10 shows f, obtained in this way, plotted against the resonator voltage, the full curve being the more exact curve deduced directly from Figure 7. It may be seen that a resonator voltage of about 130 volts is required for 50% injection efficiency.

The predominance of the factor f_1 means that the resonator voltage required for efficient synchrotron injection will increase as the voltage at which the electrons are injected into the betatron increases, since this increases V_0, e.g. about 350 volts are needed for 50% injection efficiency at an injection voltage of 100 kv.

3.2. 300 MEV. *Synchrotron*

The 300 MeV. synchrotron for Glasgow University will have $\rho_I = 7$ cm., $r_0 = 125$ cm., $E_s = 4{\cdot}5$ MeV. tentatively and 100 kv. injection voltage. The basic parameters are therefore: $V_0/v_0 = 0{\cdot}014$; $v_0 = 2{\cdot}5$ kv.; $V_0 = 34$ v.; $V_1 = 6{\cdot}3$ kv. Since $V_0/v_0 \ll 1, f_1 \simeq 1$ for all practical betatron injection voltages. The injection efficiency is therefore independent of betatron injection voltage, in contrast with the 30 MeV. machine; the fraction trapped is controlled by f_3, the $V/V_0 \gg 1$ approximation being satisfactory for all but the lowest resonator voltages, as is shown in Figure 11.

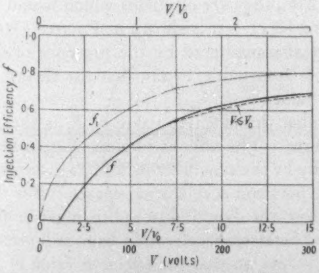

Figure 10. Injection efficiency of 30 MeV. synchrotron.

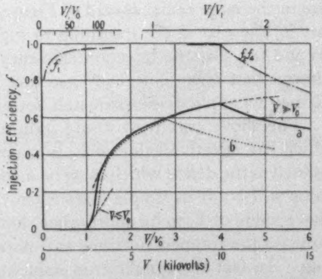

Figure 11. Injection efficiency of 300 MeV. synchrotron.
Curve a: $E_s = 4{\cdot}5$ MeV. Curve b: $E_s = 2{\cdot}5$ MeV.

In this synchrotron collision with the donut walls is important and the efficiency of trapping, $f_1 f_3$, must now be multiplied by the product $f_2 f_4$, giving a diminution in efficiency at resonator voltages in excess of 10 kv. as shown in Figure 11 curve (a).

The effect of reducing E_s to 2·5 MeV. is also shown in Figure 11 by the dotted curve (b). The corresponding values of V_0 and V_1 are $V_0 = 61$ volts and $V_1 = 3{\cdot}5$ kilovolts.

3.3. *Discussion of Examples and Limitations of Simple Theory*

The simple theory outlined has served to show that the operation of the various machines studied in the examples will be influenced by quite different factors. Before studying the experimental information which is available to warrant the approximations made, the importance of some of these approximations will be emphasized.

The main approximation made has been that the betatron action ceases suddenly and in coincidence with the turning on of the radio frequency. In fact the radio frequency is turned on in several R.F. cycles at a time when the betatron acceleration is still considerable, and the betatron acceleration is reduced quite slowly, while the resonator automatically supplies the increasing deficit required to keep the electron in the synchronous orbit.

These gradual transitions may be expected to give approximately the same effects as sudden transitions by the following argument: The resonator is switched on at a time when the volts per turn that it must supply to make up the betatron deficit is very small. The resonator voltage therefore becomes sufficient to accelerate the electrons in a time small compared with the period of the phase cycle, so that to a first approximation the R.F. may be considered as being applied instantaneously. An intermediate condition is then obtained, as shown in Figure 12(*b*), and most of the electrons are trapped, provided $V/V_0 \gg 1$. Now the betatron core begins to saturate, causing a loss of electrons as the stable area on the phase diagram shrinks, due to increase in the effective value of v_0 and therefore decrease in V/v_0. Finally v_0 obtains its nominal value with the result shown in Figure 12(*d*), and it may be seen that the fraction of electrons collected is the same as it would be if the intermediate stage of Figure 12(*b*) had been omitted. The fraction of electrons lost to the donut walls is also unaffected by the presence of the intermediate stage, for although many electrons may be lost to the walls due to the large radial spread of Figure 12(*b*), they are electrons which would be lost in any case in the transition to Figure 12(*c*). It is shown in Figures 13(*a*), (*b*) and (*c*), that the injection efficiency is also unaltered by the presence of the intermediate stage if $V/V_0 \lesssim 1$, so that it is reasonable to say that the theory of §2 may be applied approximately for all values of V/V_0.

The above argument would indicate that the effective value of E_s is that at which the effective value of v_0 is maximum. The effective value of v_0 is here defined as the deficit which must be made up by the synchrotron, and its maximum value will occur in simple cases when the betatron acceleration ceases. For the above value of E_s to be appropriate, however, the damping in radius must be the same for the trapped electrons as if normal betatron acceleration were still occurring. In fact the synchrotron damping is less, so that the effective value of E_s will lie nearer to the voltage at which the radio frequency is turned on. It is not intended to study the synchrotron damping in detail in this paper, and it will merely be assumed that the effective value of E_s lies somewhere between its value when radio frequency is turned on and its value when gamma rays appear during betatron operation. This latter value is usually quoted by experimenters, and the volts per turn supplied by the synchrotron should be approaching a maximum at this point.

A second major approximation made in the theory is that the spread of energies, or radii, on injection into the betatron, is that corresponding to the full width of the donut. If instead only a fraction Δ of the width is filled, equation (11) becomes

$$V_0=[(1-n)^2\beta_s^2E_I^2\beta_I^2(\pi k/2E_s)][\rho_I\Delta/r_0]^2. \qquad \ldots\ldots (19)$$

The fraction Δ cannot be estimated because the betatron injection process is not understood, but if synchrotron injection theory is assumed, the possibility of determining Δ experimentally arises. This will be discussed in § 4.

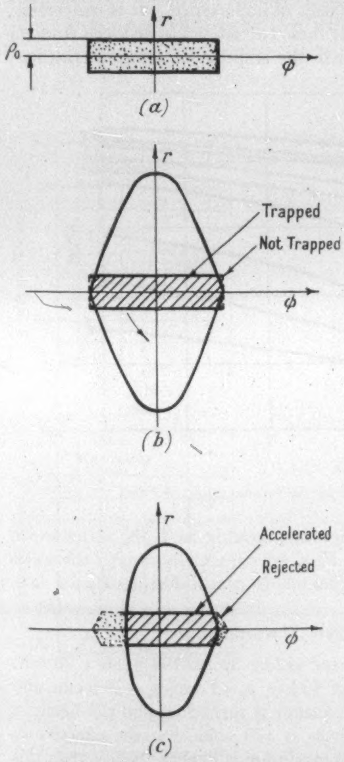
r
ρ_0
ϕ
(a)
r
Trapped
Not Trapped
ϕ
(b)
r
Accelerated
Rejected
ϕ
(c)

Figure 12. Trapping stages when V/V_0 and $V/v_0 \gg 1$.
(a) Initial condition: Betatron on, R.F. off.
(b) Intermediate condition: Betatron and R.F. on.
(c) Final condition: Betatron off, R.F. on.

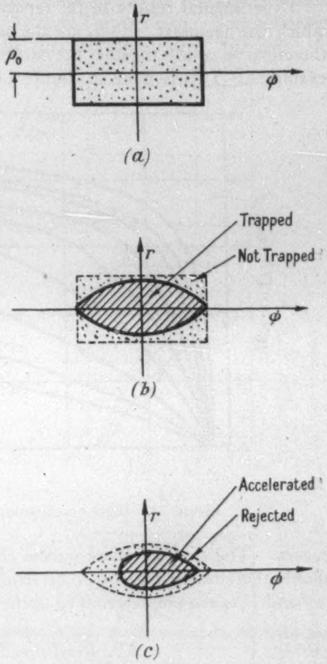
r
ρ_0
ϕ
(a)
Trapped
Not Trapped
r
ϕ
(b)
Accelerated
Rejected
r
ϕ
(c)

Figure 13. Trapping stages when $V/V_0 < 1$ and $V/v_0 \sim 1$.
(a) Initial condition: Betatron on, R.F. off.
(b) Intermediate condition: Betatron and R.F. on.
(c) Final condition: Betatron off, R.F. on.

The approximations made in the simple theory are seen to be considerable and it is not intended to support the simplifications further on theoretical grounds; clearly synchrotrons could be constructed in which the simplifications are far from justifiable, e.g. de Packh and Birnbaum (1948) have suggested such a machine. The main justification for the approximations must rest on their agreement with experiment, although it may be observed qualitatively that one would expect a simple theory of this type to give an underestimate of the efficiency.

§4. EXPERIMENTAL RESULTS

4.1. *Introduction*

Experimental results so far reported are confined to resonator voltages for which the factors f_1 and f_3 are the only ones of importance. It is convenient, therefore, to collect together the curves for these two factors as deduced from the examples. This is done in Figure 14 with the addition of some intermediary curves. The form of these curves changes appreciably as V_0/v_0 varies and it should therefore be possible to determine V_0/v_0 experimentally, even if the scales of f and V/v_0 are not determined in the experiments, as is unfortunately the case.

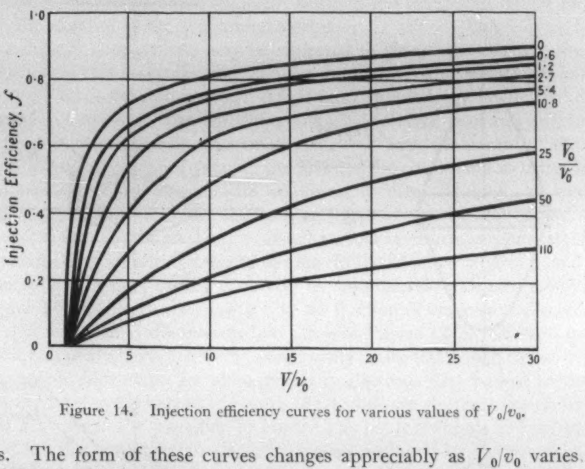

Figure 14. Injection efficiency curves for various values of V_0/v_0.

4.2. *Results on* 70 MeV. *Synchrotron*

Some measurements have been reported (Elder *et al.* 1947) on a 70 MeV. synchrotron, using an injection voltage of 40 kv., $\rho_I = 3$ cm., $r_0 = 29{\cdot}6$ cm., and $n = 0{\cdot}7$. E_s is 2·5 MeV. when the radio frequency is turned on and the betatron response appears at $E_s = 4$ MeV. v_0 is given as 170 volts, but the effective v_0 supplied by the radio frequency even at its maximum is likely to be less than this by at least 20%, due to betatron acceleration caused by leakage flux cutting the orbit. v_0 will therefore be taken as 136 volts.

The experimental results fit well a theoretical curve for $V_0/v_0 = 0{\cdot}56$ as shown in Figure 15 (*a*), and fit considerably less well a theoretical curve for $V_0/v_0 = 1{\cdot}12$, say, as shown in Figure 15 (*b*). Taking $V_0/v_0 = 0{\cdot}56$, i.e. $V_0 = 75$, and assuming $E_s = 2{\cdot}5$ MeV., Δ may be determined as 0·95 (see equation (19)). With $E_s = 4$ MeV., $\Delta = 1{\cdot}2$. The arbitrariness of the value of E_s and therefore of Δ has already been emphasized in § 3.4, but Δ may be taken as approximately unity from the above results.

4.3. *Results on 14 Mev. Synchrotron*

Some measurements have been made (Abson and Holmes 1948) on a 14 Mev. synchrotron. This synchrotron is a converted 4 Mev. betatron, requiring 1.3 volts to accelerate the electrons when the machine operates at 50 c/s., and 3.9 volts when the machine operates at 150 c/s. This low voltage occurs because the betatron gives appreciable accelerating voltage throughout the whole cycle; r_0 is 7·5 cm., ρ_I is 1·3 cm., $n=0·7$, and the operating injection voltage 10 kv. The experimental points given by Abson and Holmes are reproduced in Figure 17 (*a*). The betatron output is not negligible compared with the synchrotron output; therefore in Figure 16 (*b*) the betatron output has been subtracted from the experimental points. Further the two curves have been adjusted so that they correspond to the same betatron output and therefore to the same mean electron beam current. The curves are compared with the theory for $V_0/v_0=25$ for 50 c/s., and 8·3 for 150 c/s., and the agreement is quite satisfactory. To illustrate the accuracy of the agreement, in Figure 16 (*c*) it has been assumed that $V_0/v_0=8$ and 2·7 for the respective curves, which gives very poor fit with the experimental points.

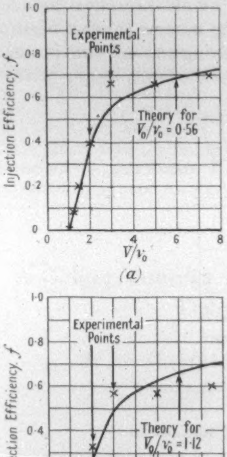

Figure 15. Experiment and theory for 70 Mev. synchrotron.
(*a*) Good fit for $V_0/v_0=0·56$.
(*b*) Poor fit for $V_0/v_0=1·12$.

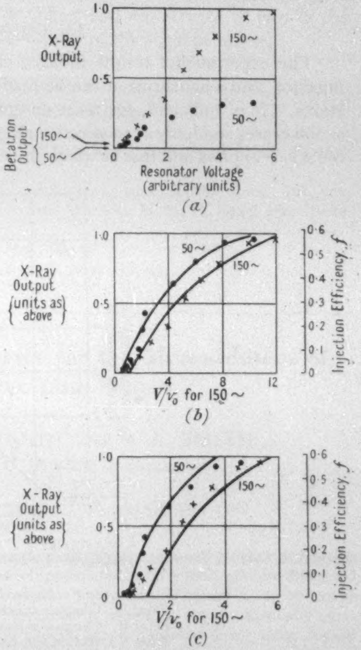

Figure 16. Experiment and theory for 14 Mev. synchrotron.
(*a*) Experimental results. (Abson & Holmes.)
(*b*) Good fit with theory if $V_0/v_0=25$ for 50 c/s. and $V_0/v_0=8·3$ for 150 c/s.
(*c*) Poor fit with theory if $V_0/v_0=8·3$ for 50 c/s. and $V_0/v_0=2·8$ for 150 c/s.

Assuming therefore, that V_0/v_0 is 25 for the 50 c/s. case, and that $v_0=1{\cdot}3$, V_0 is determined as 32·5 volts. With $E_s=2{\cdot}5$ Mev., $\Delta=0{\cdot}8$, while with $E_s=4{\cdot}5$ Mev., $\Delta=1{\cdot}0$. The value of Δ deduced from these measurements is not very reliable since the effective value of v_0 changes very slowly indeed, due to the fact that the machine is a converted betatron.

Abson and Holmes' measurements would make it possible to determine Δ more accurately than by arbitrarily assigning a value to E_s, for they made an experimental determination of the effective value of v_0 for various values of E_s. It is not intended to study their results in relation to a more comprehensive theory than that already developed here.

§ 5. CONCLUSION

The experimental results indicate that a good estimate of the efficiency of injection into a synchrotron can be made from very simple theoretical considerations. It is sufficient, for most design purposes, to assume (*a*) that betatron action ceases suddenly at an effective electron voltage lying between that at which the R.F. is applied and that at which the electrons strike the target during betatron working, and (*b*) that the donut accepts a spread of energies, during injection into the betatron, corresponding approximately to the donut width, i.e. $\Delta \simeq 1$. With these simple assumptions important differences in the behaviour of various synchrotrons, as the resonator voltage is changed, may be explained.

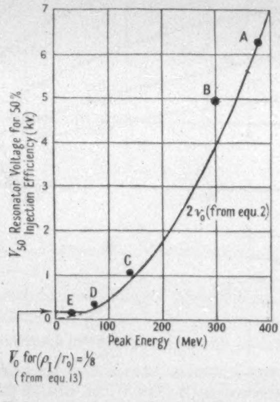

Figure 17. Resonator voltages, V_{50}, for 50% injection efficiency.
Point A: Glasgow synchrotron at 375 Mev.
Point B: Glasgow synchrotron at 300 Mev.
Point C: Oxford synchrotron at 140 Mev.
Point D: G.E. (America) synchrotron at 70 Mev.
Point E: A.E.R.E. synchrotron at 30 Mev.

It is convenient to summarize the results by a still greater simplification. For the higher energy machines the resonator voltage for 50% injection efficiency is very nearly equal to $2v_0$, as defined by equation (2), since the injection efficiency curve is very nearly curve (b) of Figure 8 for these machines, provided V/v_0 is not near unity. For the lower energy machines the resonator voltage for 50%

injection efficiency is approximately constant and equal to V_0 as defined by equation (13). Thus the required resonator voltages may be expected to follow, roughly, a curve such as that shown in Figure 17. The accuracy of this approximation is shown by the points A to E, which represent the voltages required (according to the foregoing analysis) in some actual synchrotrons.

ACKNOWLEDGMENTS

Acknowledgment is made to ideas expressed in a colloquium led by W. Walkinshaw, which directly stimulated the writing of this paper. The paper is published by permission of the Director of the Atomic Research Establishment and of the Controller H.M. Stationery Office, and was written as part of the accelerator programme of the Electronics Group of the Establishment.

REFERENCES

Abson, W., and Holmes, L. S., 1948, *A.E.R.E. Report* G/R192.
Bohm, D., and Foldy, L., 1946, *Phys. Rev.*, **70,** 249.
Elder, F. R., Gurewitsch, A. M., Langmuir, R. V., and Pollock, H. C., 1947, *J. Appl. Phys.*, **18,** 810.
Fry, D. W., Gallop, J. W., Goward, F. K., and Dain, J., 1948, *Nature, Lond.*, **161,** 504.
Goward, F. K., Wilkins, J. J., Holmes, L. S., and Watson, H. H. H., 1949, *Proc. Instn. Elect. Engrs.*, in the press.
Kerst, D. W., and Serber, R., 1941, *Phys. Rev.*, **60,** 53.
de Packh, D. C., and Birnbaum, M., 1948, *J. Appl. Phys.*, **19,** 795.

A Geiger Counter Spectrometer for the Measurement of Debye–Scherrer Line Shapes

By W. H. HALL, U. W. ARNDT and R. A. SMITH
Department of Metallurgy, University of Birmingham

Communicated by C. H. Westcott; MS. received 9th May 1949

ABSTRACT. A spectrometer for the accurate measurement of x-ray powder diffraction line intensities and shapes is described. Monochromatic radiation is used, and the diffracted beam intensity is recorded by a Geiger counter. The intensity of the x-ray source is monitored continuously, and errors due to variations in its output are automatically compensated. The accuracy and resolution obtainable are demonstrated by some typical experimental results.

§1. INTRODUCTION

THE accurate measurement of the shapes and intensities of x-ray diffraction lines from powders has long been an important problem. In this country the most common experimental arrangement involves the use of a specimen in the form of a thin rod placed at the centre of a cylindrical camera (Bradley, Lipson and Petch 1941) and the subsequent densitometry of the photographic record. In another technique, that used by Brentano (1925, 1937) and by Brindley and Spiers (1934), the specimen is in layer form and side reflections from the surface are used. The arrangement has the advantage that a beam some degrees in aperture may be employed; the use of a focusing monochromator (Smith and Stickley 1943) eliminates the need for the prohibitively long exposures which are required when orthodox cylindrical cameras of comparable resolution are used in conjunction with plane crystal monochromators. The side reflection method has the additional advantage for accurate work that the corrections for absorption in the specimen can be made with greater precision than in the case of a cylindrical specimen.

The spectrometer to be described retains the geometrical arrangement of focusing monochromator and side reflection from a powder layer. The intensity of the diffracted x-ray beam is measured directly and instantaneously by a Geiger counter, thereby eliminating the photographic film and the difficulties of maintaining standard conditions of processing and of densitometry. The Geiger counter method offers considerable advantages in speed, especially where changes in only one or a few lines are to be studied; this factor is important in metallurgical applications since comparatively rapid phase changes can be investigated.

§2. THE SPECTROMETER

The geometry of the spectrometer is shown in Figure 1. A curved quartz crystal monochromator M rigidly mounted on the x-ray tube provides a monochromatic beam of two or three degrees aperture diverging from S_1, the entrance slit of the spectrometer. The powder block P, which is rotated continuously in its own plane, is set so that the angle between its surface and the incident x-ray beam is the Bragg angle for the line under investigation. The diffracted beam is then focused on to an adjustable slit S_2 behind which is a Geiger counter G. The slit and Geiger counter are mounted on an arm which may be rotated about the centre of P in such a way that the line joining the centre to S_2 makes an angle with the plane of the specimen which is equal to the angle of incidence. Thus the counter arm is rotated about the vertical axis through the centre of the spectrometer at twice the speed of the specimen; for any setting the circle through S_1 and S_2 tangential to P is the focusing circle (Brentano 1937). Soller slits A and B, limiting the vertical divergence of the beam to 1°, may be added when required (Alexander 1948).

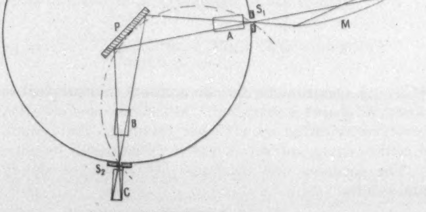

Figure 1. Geometry of spectrometer.

The base of the instrument is that of a commercial ionization spectrometer (Wooster and Martin 1936), supplied by Unicam Instruments Ltd. of Cambridge.

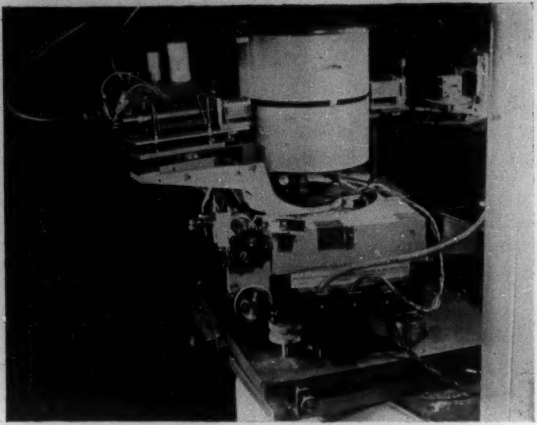

Figure 2. The spectrometer.

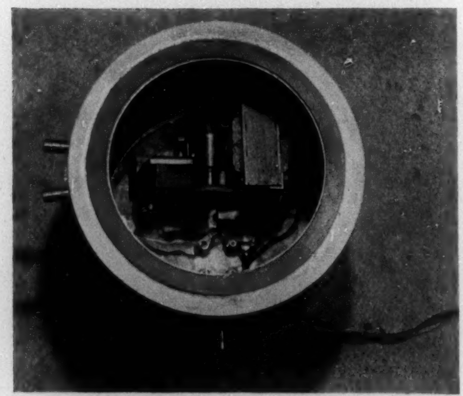

Figure 3. The specimen assembly.

Two concentric tables, one carrying the specimen chamber and the other the Geiger counter arm, can be rotated independently by spring-loaded worm drives or geared together so that the angular rotation of the arm is double that of the specimen table. The angular positions of each can be read on drums calibrated in minutes of arc, an overall accuracy of two minutes being claimed. Considerably greater accuracy is obtainable in measuring small angular differences.

The adjustable entrance slit (Barnes and Brattain 1935) is mounted on a pillar so arranged that scanning of the counter arm up to $2\theta = 165°$ is possible.

The attainable resolution is limited by the radius of the spectrometer, the slit widths, the lack of perfect focusing, and the vertical divergence of the x-ray beam. A spectrometer radius of 11·46 cm. is convenient since a change in Bragg angle of one degree then corresponds to a traverse of S_2 of exactly 4 mm. The minimum counter slit width found in practice to be compatible with a reasonable counting rate is 0·1 mm.; this subtends an angle of three minutes at P. Perfect focusing at S_2 would be obtained only if the surface of the powder layer coincided with the focusing circle S_1PS_2 (Figure 1). However, for beams of about 2° aperture, the loss of resolution caused by a flat specimen is inappreciable (Brindley 1935). When maximum resolution is required, the vertical divergence of the x-ray beam may be limited by Soller slits, but the available intensity is considerably reduced. It should be noted that when a monochromator is used the small angular separation between the α_1 and α_2 components of the beam entering the spectrometer may either increase or decrease the doublet separation after diffraction by the specimen. All our measurements are carried out on that side of the beam where the dispersions are additive, thus effectively increasing the $\alpha_1\alpha_2$ resolution.

§ 3. THE SPECIMEN CHAMBER

Experiments have shown that it is difficult to reproduce accurately all the settings of the spectrometer in such a way that after readjustment identical counting rates are obtained for the lines from a given sample. Substances under investigation are therefore compared with a standard reference specimen. The sample holder is a bakelite disc, 2¼ inches in diameter, having an inner circular recess ¾ inch in diameter and an outer annular recess into which sample and reference powders respectively are packed. A small electric motor rotates the disc by a friction drive on its outer rim. The assembly is mounted on an arm which can be tilted about a horizontal axis normal to the plane of the specimen. The throw is limited by two stops so that in one position the x-ray beam strikes the inner sample while in the other it falls on the outer reference specimen; tilting is effected by a mains-operated solenoid. The entire mechanism is mounted in a cylindrical chamber which can be evacuated or filled with hydrogen when necessary, since the absorption of x rays in a 20 cm. air path varies from about 20 per cent for CuKα to 55 per cent for CrKα radiation. X rays enter and leave the chamber through a 180° slot covered with 'Cellophane', the top being closed by a glass plate and rubber gasket. Three legs allow levelling and height adjustment and locate the specimen chamber accurately on the spectrometer by means of a hole, slot and plane. A screw adjustment to bring the surface of the specimen exactly over the centre of the spectrometer is also provided. The specimen chamber is shown in position on the spectrometer in Figure 2; Figure 3 shows details of the specimen disc assembly inside the chamber.

§4. THE GEIGER COUNTER

The counters used in our work are all cylindrical argon-alcohol counters (Friedmann 1945), the x rays entering through an aperture in the front face as close as possible to the axis. The anode wire, which is of 0·1 mm. diameter tungsten, is supported at both ends, care being taken to reduce the dead volume at the front end as much as possible. In view of the high filling pressure used (50 cm. Hg), this latter point is important in order to avoid unnecessary absorption in this dead space. The entrance aperture is covered with 0·01 mm. aluminium foil, and the active length is about 12 cm. The calculated efficiency, i.e. that fraction of the x-ray beam incident on the counter which is absorbed in the active length, ranges from 50 per cent to 65 per cent for wavelengths from CuKα to CrKα. The starting potential of this counter is about 1600 volts and its dead time is about 200 microseconds.

§5. CIRCUITS

The circuits used are all conventional, the arrangement being shown diagrammatically in Figure 4. The output from the measuring counter is first fed into a quenching circuit arranged immediately adjacent to the counter on the counter arm (Figure 2)*. While the use of an external quenching circuit slightly lengthens the resolving time of the system, it improves the plateau and increases the counter life; in addition, the counting characteristics become less dependent on temperature and previous treatment of the counter. We have used circuits of the Neher–Harper type (1936) and of the Getting type (1938) with equal success. A cathode follower output feeds the pulses into cables leading to the measuring circuits.

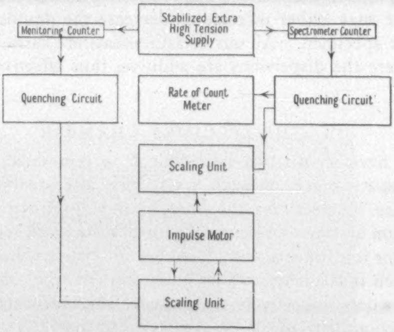

Figure 4. Schematic circuit diagram.

The pulses are fed either into a scale-of-100 scaling unit (Rotblat, Sayle and Thomas 1948) for accurate measurements, or into a simple integrating circuit (Evans and Alder 1939). The latter has been found very useful during alignment of the apparatus and for rapid surveys of the diffraction pattern of a sample.

---

* For Figures 2 and 3 see Plate.

The stabilized E.H.T. supply for the counter follows orthodox design. It contains two independent continuously variable outputs, the one used for the spectrometer counter, the other for a second counter monitoring the X-ray output of the tube.

§6. THE MONITOR UNIT

In X-ray diffraction work in which all parts of the pattern are recorded simultaneously on one strip of film, no special precautions are necessary to keep constant the X-ray output of the tube. The use of a spectrometer of the type described, in which the spectrum is scanned by a moving counter, demands either a rigid stabilization of the characteristic X-ray output of the tube or a continuous monitoring of the same, since the scanning of all the lines of a given sample occupies a period of some hours. The latter method was adopted in our work. A plane quartz crystal monochromator is mounted opposite the second window of the X-ray tube; the characteristic radiation from this is allowed to fall on a copper wire. The diffracted rays from the latter are received by a second Geiger counter with its own quenching circuit and scaling unit. In parallel with its Post Office message register the latter drives an impulse motor which breaks a pair of contacts after receiving 104 pulses, i.e. after 10,400 pulses have been registered by the monitoring counter. The contacts operate a relay which switches off both the counting and the monitoring scalers. Consequently, the diffracted intensity is measured, not for a fixed time interval, as in normal practice, but for a fixed quantity of energy emitted by the X-ray tube. The recorded intensity has been found to be virtually independent of X-ray tube current, and voltage fluctuations less than 50 per cent. Any variations outside this range may be due to changes in the focal spot of the X-ray tube which affect the two windows unequally and to differences in the counting losses when the intensity changes greatly.

The counting time can be conveniently adjusted by varying the length of the copper wire bathed by the monochromatic beam by means of an adjusting screw.

§7. AUTOMATIC DRIVE

To accelerate the scanning of a line we have fitted a geared motor drive to the spectrometer worm shaft, the motor being energized through a pair of contacts bearing on a disc attached to the shaft. The disc carries at predetermined angular intervals a number of bosses which break the motor circuit when the contacts come opposite them. The motor is started by a push button connected in parallel with the contacts; it is stopped by the opening of the contacts after the spectrometer spindle has turned through the appropriate angular interval. Provision of two field windings on the motor allow it to be operated in either direction.

The process of scanning a line is thus reduced to the operation of two push buttons. Pressing the first starts the count, which stops after 10,400 pulses from the monitoring counter; pressing the second resets the scaler and moves on the spectrometer to the next position.

§8. USE OF THE INSTRUMENT

In order to illustrate the setting-up and the operation of the instrument the steps necessary for recording the spectrum of a sample under investigation will now be described.

The monochromator having been adjusted to give a beam of the required aperture, the spectrometer is placed on its table and moved until its entrance slit is at the focus of the monochromator and the beam passes over the exact centre of the spindle. It is convenient to use a centre locator for this purpose, consisting of a vertical rod mounted on a table which can be placed on the spectrometer. The shadow of this rod is observed on a fluorescent screen as the spectrometer is moved into the beam.

The counter is fixed on its table and levelled. The counter arm is swung into position to receive the direct x-ray beam, a sufficient number of absorbing screens being placed in front of the counter entrance slit to prevent the counter from saturating. It is turned about its entrance slit until the indication on the counting rate meter is a maximum. Both sets of Soller slits are now placed in position if required and, after approximate levelling with the aid of a fluorescent screen, they are adjusted for a maximum meter reading.

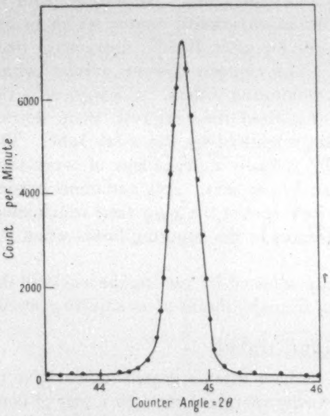

Figure 5. Aluminium line 4.
CuKα 50 kv., 10 ma. G-M slit = 0·2 mm.

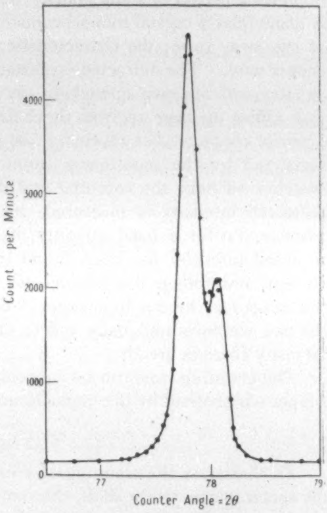

Figure 6. Aluminium line 11.
CuKα 50 kv., 10 ma. G-M slit = 0·2 mm.

The specimen chamber is placed in position and the specimen is brought over the centre spindle, using a microscope for this purpose. The specimen table is turned to the focusing angle (Figure 1) and the two spindles geared together.

The counter entrance slit is set to the required width and the specimen motor switched on.

A preliminary scan of the spectrum is made, using the counting rate meter to determine the positions and the approximate intensities of the lines. The monitor is now set for an appropriate counting time and the spectrum is scanned accurately, using the scaler.

After every line is scanned comparison counts are taken on the reference specimen, both as a check on the stability of the measurements and to enable them to be placed on an absolute intensity scale if required. When the peak counting rate on any line exceeds 20,000 counts per minute one or more absorbing screens are placed in front of the counter since, for intensities greater than this, corrections for counting losses become too great to be accurately determinable.

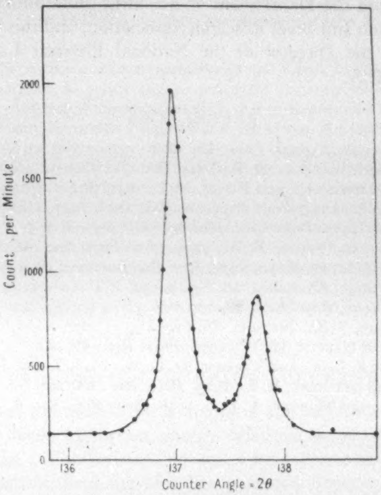

Figure 7. Aluminium line 24.
CuKα 50 kv., 10 ma. G-M slit=0·2 mm.

The time spent in any one position is determined by the required accuracy (Hall 1949). The standard deviation of a single observation is $[n_1+n_1^2/n_2]^{\frac{1}{2}}$, where n_1 is the number of pulses from the specimen and n_2 that from the monitoring counter.

§ 9. TYPICAL RESULTS

Figures 5, 6 and 7 are typical records of aluminium diffraction lines 4, 11 and 24 using CuKα radiation at 50 kilovolts and 10 milliamperes. The resolution, contrast and small scatter of individual readings, particularly of the background, compare well with microphotometer traces of films. Replacement of the Geiger counter by films showed exposure times of several hours to be necessary under these conditions, whereas the counter records were obtained in times of thirty to sixty minutes each, depending on the angular separation of the Kα doublet. Faster scanning can only be carried out at a sacrifice of accuracy, which in these experiments was sufficient to make the standard deviation of the integrated intensity about one per cent.

ACKNOWLEDGMENTS

It is a pleasure to acknowledge the encouragement given to us by Professor D. Hanson. We have had valuable discussions on the design of the circuits with Mr. C. Wainwright of the National Physical Laboratory, and with Mr. D. Bracher and Mr. A. Ward. The help of Mr. C. Ramm in the construction and filling of counters is gratefully acknowledged, as is the assistance of Mr. G. K. Williamson in the later stages of the work. The work was undertaken under research grants from the Department of Scientific and Industrial Research and from the British Iron and Steel Research Association, and this paper is published by permission of the Director of the National Physical Laboratory and the Director of B.I.S.R.A.

REFERENCES

ALEXANDER, L., 1948, *J. Appl. Phys.*, **19**, 1068.
BARNES, R. B., and BRATTAIN, R. R., 1935, *Rev. Sci. Instrum.*, **6**, 83.
BRADLEY, A. J., LIPSON, H., and PETCH, N. J., 1941, *J. Sci. Instrum.*, **18**, 216.
BRENTANO, J. M. C., 1925, *Proc. Phys. Soc.*, **37**, 184; 1937, *Ibid.*, **49**, 61.
BRINDLEY, G. W., 1935, *Proc. Leeds Phil. and Lit. Soc.*, **3**, 353.
BRINDLEY, G. W., and SPIERS, F. W., 1934, *Proc. Phys. Soc.*, **46**, 841.
EVANS, R. D., and ALDER, R. L., 1939, *Rev. Sci. Instrum.*, **10**, 339.
FRIEDMANN, H., 1945, *Electronics*, **18**, No. 4, 132.
GETTING, I. A., 1938, *Phys. Rev.*, **53**, 103.
HALL, W. H., 1949, *J. Sci. Instrum.*, **26**, 61.
NEHER, H. V., and HARPER, W. W., 1936, *Phys. Rev.*, **49**, 940.
ROTBLAT, J., SAYLE, E. A., and THOMAS, D. G. A., 1948, *J. Sci. Instrum.*, **25**, 33.
SMITH, C. S., and STICKLEY, E. E., 1943, *Phys. Rev.*, **64**, 191.
WOOSTER, W. A., and MARTIN, A. J. P., 1936, *Proc. Roy. Soc.* A, **155**, 150.

Surface Forces in Liquids and Solids

By C. GURNEY
Engineering Laboratory, Cambridge University

MS. received 27th May 1948, *and in amended form* 1*st April* 1949

ABSTRACT. The author's recent treatment of the forces in the surfaces of liquids is extended to the surfaces of solids and to interfaces between solids and liquids. Solid surfaces formed by cleavage at temperatures such that no appreciable migration of molecules takes place, will usually be under a state of uniform stress, not necessarily tensile and not numerically equal to the free energy of the surface. If appreciable atomic migration takes place, the surface of a crystalline solid melts, and the solid is covered with a thin liquid film under a tension force greater than that of the corresponding supercooled liquid, and such that the chemical potential of the molecules in the liquid film is equal to that of molecules in the crystal. This tension force is numerically equal to the free energy of the surface. If such a solid is subsequently cooled to a temperature at which atomic migration effectively ceases, it will have frozen in its surface a tension force corresponding to thermal equilibrium at some higher temperature. The Laplace Q force is discussed in terms of modern theories of atomic bonding and applied to the case of equilibrium at angle of contact between solid and liquid.

---

§1. INTRODUCTION—SURFACE FORCES IN LIQUIDS

THE idea that the tension force acting in the surface of liquids is a fiction whose use leads to correct energy relations is very commonly met with in textbooks. The fictitious nature of the force appears to have been first suggested by Laplace, and the idea has persisted because of the failure until recently to account for the force in terms of the position and motion of molecules.

In a recent paper, Brown (1947) has criticized the prevalent textbook treatment and has explained the presence of the tension force in the surface of liquids by a simple argument. In the discussion of Brown's paper, and more fully in a later paper (Gurney 1947), the present author has explained the tension in terms of the position and motion of molecules by giving a molecular interpretation to the thermodynamics of surfaces as developed by Gibbs. Gibbs showed that, at all parts of a system in equilibrium, whether homogeneous or not, the intrinsic or chemical potential μ of each species of molecule present must have a constant value; μ is defined by

$$dE = TdS + dW + \Sigma \mu dn,$$

where E is energy, T temperature, S entropy, W work ($=\gamma dA$ for surfaces free from pressure) and n is the quantity of substance. If μ has not a constant value, then molecules migrate from parts of the system where μ is high, to parts where μ is low, until equality of μ is achieved. The μ of molecules depends on their relative arrangement. At a surface not acted upon by a tension force (stress-free surface), because of their unsymmetrical environment, the μ of surface molecules would exceed that of interior molecules, and more molecules would therefore leave the surface region than would enter it, leaving fewer molecules to occupy the given area. The molecules remaining in the surface are therefore at a spacing exceeding the stress-free spacing and there is consequently a tension force between them. The tension force reduces the μ of surface molecules according to the relation

$$(\partial\mu_i/\partial\gamma)T, n = -(\partial A/\partial n_i)T, \gamma, n_r, \qquad \ldots\ldots (1)$$

where μ_i and n_i are the chemical potential and number of molecules of the species i at the surface. γ is the tension force per unit width, and A is area. This expression can be derived from the expression for dE by changing the independent variables to T, γ, and n, and then equating the crossed differentials of the coefficients of $d\gamma$ and dn.

Equilibrium is achieved when, due to continued depopulation of the surface, the tension force reaches such a value that the μ of surface molecules equals that of interior molecules. Where more than one species of molecule is present, the variation of the single variable of surface tension force is not sufficient to ensure the equality of the μ of each species of molecule at the surface and in the interior. The proportion of different species of molecules at the surface must also vary, and at equilibrium it differs from that in the bulk phase (Gibbs adsorption).

When dealing with interfaces between immiscible liquids a clearer physical picture can be obtained if the force in the plane of the interface is regarded as composed of two parts, the force between molecules of phase A at an interface with phase B being written γ_{Ab} and that between molecules of B at an interface with A being written γ_{Ba}. These forces are conveniently called partial interfacial forces. Their sum is the total force in the interface γ_{AB}. This procedure applied to interfaces between solid and liquid was made use of by Gibbs (1876) and Kelvin (1886). It has recently been advocated by Brown (1947). It is applied here to interfaces between two liquids. Equation (1) then applies to the partial interfacial forces as well as to forces at free surfaces. The partial interfacial force of the phase A is that necessary to cause the μ of phase A molecules at the interface to equal that of phase A molecules in the bulk liquid. Because of the positive work of cohesion between all substances, the presence of phase B will cause the μ of stress-free phase A molecules at the interface to be less than that of stress-free molecules at a free surface. The partial interfacial force γ_{Ab} will therefore be less than the tension γ_{A} at a free surface. Similar considerations apply to γ_{Ba}. If there is strong cohesion between A and B molecules, one of the partial interfacial forces may be compressive, but for stability the total interfacial force between liquids must be tensile.

In the case of a liquid covered by a monolayer which is not in equilibrium with a bulk phase, the partial interfacial force between monolayer molecules is not decided by considerations of thermal equilibrium, but may have any value depending on the area in which the monolayer molecules are constrained to occupy. The partial interfacial force of the underlying liquid will be decided by considerations of thermal equilibrium, and will vary in a definite way with the spacing of the monolayer molecules. The usual method of regarding the forces between monolayer molecules as equal to the difference between the total surface when the monolayer is present and the tension in the free surface of the underlying liquid when not covered by monolayer is not strictly correct. This method always leads to compressive forces between monolayer molecules, whereas at suitable larger molecular spacings a tension force would be expected.

The ideas of Laplace which were later extended by Rayleigh and Bakker do not, as these authors suggest, explain the tension force in the surfaces of liquids, because they have not introduced the interchange between surface and interior molecules which is fundamental to the correct explanation. Laplace gave two treatments of the forces in surfaces. The first, which finds a frequent place in textbook treatments, is an extension of ideas first published by Young (1805), and leads to the conclusion that the interior of a body is acted upon by an "intrinsic pressure" of magnitude $K+H/r$ where r is the radius of curvature of the surface.

Laplace considered that the term H/r explained the rise of liquid in a capillary. We have already seen that a static theory such as this does not apply to liquids because interchange of molecules is not taken into account. The equilibrium of liquids under a curved surface is readily explained by the liquid having the real tension which results from the thermodynamic theory. The idea of intrinsic pressure does not lead to any very ready explanation of any of the phenomena discussed in this paper, and we shall not consider it further. For an account of Bakker's extension of the intrinsic pressure theory the reader is referred to the paper by Brown (1947). Bakker's theory does not lead to Gibbs adsorption at the surface of a multicomponent liquid, and if only for this reason it cannot be regarded as correct.

In addition to his intrinsic pressure theory Laplace (1807) gave in his *Nouvelle manière de considérer l'action capillaire* an explanation of the forces between the walls of a capillary tube and the liquid contained in it which does not receive the attention it deserves from modern writers. In §4, when dealing with surface forces in solids, and later, when discussing angles of contact, we shall make use of this theory.

§2. STRESSES IN THE UNCONTAMINATED SURFACES OF SOLIDS AT TEMPERATURES AT WHICH MIGRATION OF ATOMS TAKES PLACE

At temperatures far below the melting point migration of atoms takes place at a negligible rate and the attainment of thermal equilibrium between surface and interior will be indefinitely delayed. At higher temperatures appreciable atomic migration takes place even in the crystalline state. Evidence for this comes from the conductivity of ionic crystals and the diffusion of solute ions in metals. At such temperatures, possibly after considerable delay, thermal equilibrium between surface and interior will be achieved and the μ of surface atoms will then equal that of interior atoms.

Consider first the case of the surface of a liquid. If we imagine a liquid to have a stress-free surface, then the μ of surface molecules is higher than that of interior molecules and an excess of molecules enters the interior, increasing the volume of the bulk phase and leaving fewer molecules in the surface to occupy the given area. The spacing of surface molecules thus exceeds the equilibrium spacing and a tension stress in the plane of the surface is set up. This tension has the effect of reducing the μ of surface molecules according to equation (1). The tension stress therefore tends to prevent molecules leaving the surface. The manner in which this is effected is illustrated in Figure 1 which represents three stages in the escape of a molecule from the surface into the interior or into the vapour phase.

It is seen that because the liquid molecules cohere to each other and, being mobile, close the hole which would otherwise be formed, the tension during stage 1 of the process of escape tends to pull the escaping molecule back into the surface. Equilibrium is achieved when, due to the continued inward migration of molecules, the tension becomes equal to the value which makes the μ of the surface equal to the μ of the interior.

Consider now the stress-free surface of a crystalline solid at a temperature such that atoms can migrate. Let us suppose that initially all the lattice points are occupied by atoms. Then just as in the case of a liquid, more atoms leave the surface than enter it, the inward migration of atoms being accommodated by an appropriate increase in the number of interior lattice points. At this stage the remaining surface atoms would still be on lattice points but there would be a number of vacant sites. The entropy of surface atoms would be increased but this does not effect μ because $(\partial\mu/\partial S)_{\gamma T}=0$. If this state of affairs persisted, no effective tension would be set up in the surface, and atoms would continue to leave the surface; thermal equilibrium would be impossible. For thermal equilibrium, it is necessary that the departure of atoms from the surface should set up a force opposing further departure. What is the nature of this force?

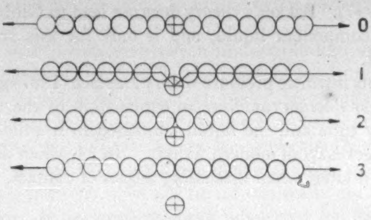

Figure 1.

At any temperature below the melting point of a crystalline solid thermal equilibrium requires that there should be some interior vacant lattice sites. As the temperature is raised the number of these vacant sites increases and above the melting point the solid phase with its vacant lattice sites is unstable with respect to the liquid phase. The solid therefore melts. We have just seen that an initially perfect surface of a solid would lose atoms to the interior and that there would be an increasing number of vacant lattice sites at the surface. When these reach a given number it is reasonable to expect that the crystalline arrangement of surface atoms will become unstable with respect to the liquid arrangement and the atoms at the surface will melt, forming a liquid film a few atoms thick which completely covers the surface. Thermal equilibrium between surface and interior then becomes possible.

If the liquid film when formed were stress free, atoms would continue to leave the surface until a tension stress was set up in the liquid film such that the μ of atoms in the liquid film was equal to the μ of interior atoms. As the liquid film is in equilibrium with the solid phase at a temperature below the melting point of the latter, it follows that the tension in the liquid film must be higher than that in the surface of the corresponding supercooled liquid phase. The necessary value of the tension can be estimated as follows. The equation corresponding to equation (1) for a bulk phase is

$$\partial\mu/\partial p=\partial V/\partial n, \qquad \ldots\ldots(2)$$

where p and V are pressure and volume.

At the melting point the μ's of solid and liquid bulk phases are equal and at all temperatures the μ's of solid and liquid must equal those of the corresponding vapour phases so that the difference in the μ's of the solid and liquid bulk phases at temperature T is given by

$$\Delta\mu=\Delta\int_{p}^{p_{\text{melting}}}\frac{\partial V}{\partial n}\,dp, \qquad \ldots\ldots(3)$$

where p is vapour pressure.

Assuming the vapours to be perfect gases this becomes

$$\Delta\mu=\boldsymbol{R}T\ln p_{\mathrm{L}}/p_{\mathrm{S}}, \qquad \ldots\ldots(4)$$

where the subscripts L and S stand for liquid and solid.

Integrating equation (1) and neglecting variation in $\partial A/\partial n$,

$$\Delta\mu=-\frac{\partial A}{\partial n}\,\Delta\gamma. \qquad \ldots\ldots(5)$$

Equation (4) gives the difference between the μ of solid and liquid bulk phases. Equation (5) shows how the μ of a liquid surface phase is altered by tension. If we are to have a liquid surface phase in equilibrium with a solid phase the μ's of the phases must be equal. Using equations (4) and (5) we must therefore have

$$\boldsymbol{R}T\ln p_{\mathrm{L}}/p_{\mathrm{S}}-\frac{\partial A}{\partial n}\,\Delta\gamma=0 \qquad \ldots\ldots(6)$$

or

$$\Delta\gamma=\frac{\boldsymbol{R}T\ln p_{\mathrm{L}}/p_{\mathrm{S}}}{\partial A/\partial n}. \qquad \ldots\ldots(7)$$

Chalmers, King and Shuttleworth (1948) have estimated the ratio of $p_{\mathrm{L}}/p_{\mathrm{S}}$ for silver for the temperature range between the melting point (961° c.) and 600° c. At 600° c. $p_{\mathrm{L}}/p_{\mathrm{S}}=1{\cdot}42$. $\partial A/\partial n$ is the effective area occupied per molecule and for silver is roughly 10 A^2. Using these data the value of $\Delta\gamma$ is estimated to be about 40 dynes/cm. The surface tension of the supercooled bulk liquid at 600° c. would be of the order of 1,000 dynes/cm. so that it is seen that in this case quite a small increase in tension is sufficient to enable a liquid film to be in equilibrium with a bulk crystalline phase at temperatures well below the melting point. For ice at -15° c. the ratio $p_{\mathrm{L}}/p_{\mathrm{S}}$ is 1·15 and $\partial A/\partial n$ is about 5 A^2. These figures give a value for $\Delta\gamma$ of approximately 10 dynes/cm. The surface tension of water at -15° c. is about 80 dynes/cm. so that the tension in the liquid film on the surface of ice at this temperature is about 90 dynes/cm. This means that ice at -15 °c. should rise appreciably higher in a capillary tube than liquid water at the same temperature. The effect is extra to the ordinary density effect.

The mobility of surface atoms of solids at temperatures well below the melting point is a well known phenomenon, and is made use of in the sintering of powders. An account of a number of effects associated with the mobility of atoms on surfaces of metals is given by Chalmers *et al.* (1948). Many of the effects may be explained by the presence of liquid films on the surfaces of crystals, and the fact that crystals cannot be superheated above their melting points is readily understood if even below the melting point the solid already has a film of liquid on it. A bulk liquid phase becomes stable at a temperature such that the tension in the liquid film on the solid is equal to the tension in the bulk liquid phase. The liquid film on ice probably plays an important part in skating.

Frenkel (1945) has considered the subject of surface mobility from a statistical mechanical point of view. He has regarded the surfaces of crystals as having the same atomic arrangement as that of the interior atoms, and has then estimated the number of adsorbed individual atoms which would rest on the top of the surface. He regards these adsorbed atoms as being the source of surface mobility. In his paper he does not apply the statistical mechanical argument to the thermal equilibrium between the surface and the interior of the crystal. If this were done, because surface atoms are in a state of high potential energy, the statistical mechanical argument would presumably predict that they would be less closely packed and would lead to a liquid film on the surface just as the thermodynamic argument does. The isolated movable atoms of Frenkel would then move about on the top of the liquid surface, but they would be too few compared with the number of atoms in the liquid film to play any important part in surface mobility phenomena. They would, however, play an important part in evaporation, the atoms going first to the top of the surface and then later being thrown off.

§3. UNIFORM STRESSES IN UNCONTAMINATED SURFACES OF SOLIDS AT TEMPERATURES AT WHICH MIGRATION OF ATOMS DOES NOT TAKE PLACE

In solids at temperatures at which no appreciable migration of atoms takes place, a state of thermal equilibrium between surface and interior is not reached, and the process by which the tension force in the surfaces of the liquids is set up does not operate. There will, nevertheless, be uniform stresses acting in the freshly cleaved surfaces of such solids due to the fact that the stress-free spacing of surface atoms differs from that of interior atoms. In the case of liquids, the surface forces are brought to equilibrium at the perimeter by forces between the surface atoms and the walls of the containing vessel. In the case of solids with non-mobile atoms the surface stresses are brought to equilibrium by shear forces between surface and underlying atoms—a state of internal stress is set up near the surface. The detailed explanation of such surface stresses will depend on the predominant type of atomic bonding, covalent, ionic or metallic. To illustrate their nature consider a material having ionic bonding, where each positive ion is surrounded by negative ions and vice versa. Pauling (1940, p. 368) gives a table showing how equilibrium interatomic distances in solids vary with coordination number (number of nearest neighbouring atoms). For positive and negative atoms in a three-dimensional chess-board pattern, the coordination number is six in the interior of the solid but only five at the surface. For this case, Pauling gives the reduction in interionic distance with reduction in coordination to be about four per cent. Lennard-Jones and Dent (1928) have calculated the equilibrium spacing of a two-dimensional array of positive and negative ions, and they find it to be of the order of 5% less than the equilibrium spacing in the bulk phase. The difference, for their calculation, is due to the fact that there is less mutual repulsion between ions of like sign in a two-dimensional than in a three-dimensional array. They have not taken into account the difference in the distribution of electron densities for the plane and for the solid arrays of atoms.

This effect is additional, but the combined result may not be simply additive. The cube surfaces of an ionic bonded material would therefore be in a state of tension relative to the interior, but this would not apply to all surfaces. A surface formed by a 111 plane would contain only ions of like sign, and the mutual repulsion of these would result in a surface having a compression stress in its plane.

Such uniform stresses in surfaces bear no immediate relation to the work of cohesion, so that it is misleading to call these stresses surface tensions. We shall refer to them as induced tangential stresses; they do not play any very direct part in the surface phenomena discussed.

In this section it has been assumed that the surface has been formed at low temperature by mechanical means. If it has been formed by cooling an existing surface from a temperature so high that appreciable atomic migration took place, then it will have a uniform tension frozen into it, corresponding to the equilibrium tension at some higher temperature.

§4. THE LAPLACE *Q* FORCE AND EQUILIBRIUM AT ANGLES OF CONTACT

If two blocks of material are placed in partial contact as in Figure 2(*a*), there will be local tangential forces between them, tending to cause relative sliding so that the surfaces on which sliding takes place are eliminated and the two blocks become one.

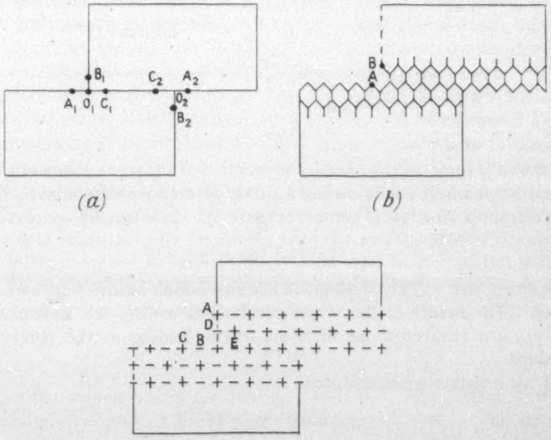

(*a*) (*b*)

(*c*)

Figure 2.

The tangential forces arise from the tangential components of the cohesive forces between the blocks. On Laplace's model of matter they are explained as follows. The attraction of a particle at C_1 (see Figure 2(*a*)) for a particle at B_1 is balanced by the intrinsic pressure, so that there is no tendency for the distance B_1C_1 to shorten. The attraction of a particle at A_1 for a particle at B_1 acts across space and is unbalanced. There is therefore a resultant tangential force acting in the region of O_1 tending to cause relative sliding of the blocks. There is a similar force at O_2. We will call these forces the Laplace tangential cohesive forces and denote them as Laplace did by Q. On more modern ideas of the composition of matter, the explanation of the force Q must be given in terms of the predominant type of atomic bonding. In Figure 2(*b*) is a picture of a solid considered as two-dimensional in which for simplicity each atom forms three covalent bonds. In this case the surface atoms will have a free valency and the tangential cohesive force would come from the stretched covalent bond formed between atoms A and B.

In an ionic bonded material shown in Figure 2(*c*) the tangential cohesive force would arise from attractive forces between ions such as A and B and C and D which act across space not occupied by other ions; and also from polarization (Lennard-Jones and Dent 1928) of the ions B and D which would result in less repulsion between ions B and D than between ions D and E.

Because in an isothermal process, the minimum work to cause a given change is independent of the path, each force Q is equal to one half of the work of cohesion, since new surfaces may be formed either by normal separation or by sliding. It should be noted that the Laplace Q force is a local force acting at the junction between the free surface and a bulk phase and does not cause a stress to be set up over the whole of the free surface.

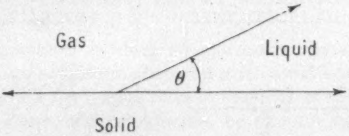

Figure 3.

A Laplace Q force will also act at the junction of the free surface of a solid and liquid in the case where a solid surface is partly covered with the liquid. Consider the equilibrium at an angle of contact (Figure 3). It is usually written

$$\gamma_{LG}\cos\theta+\gamma_{LS}-\gamma_{SG}=0, \qquad \ldots\ldots (8)$$

where γ_{LG}, γ_{LS} and γ_{SG} are tensions in the gas–liquid, liquid–solid and solid–gas interfaces. The nature of the forces involved is usually left unexplained and γ_{LS} and γ_{SG} are referred to as fictitious forces leading to the correct energy relationships.

With our notation we should write

$$\gamma_{Lg}\cos\theta+\gamma_{Ls}-Q=0, \qquad \ldots\ldots (9)$$

where γ_{Ls} is the partial interfacial force (not necessarily tension) necessary to enforce equality of the μ's of molecules of the liquid at the interface and of molecules in the bulk liquid, and Q is the Laplace tangential cohesive force.

If the solid is at such a temperature that a liquid layer is formed on its surface equation (8) applies, all the forces being real forces necessary to ensure the various equalities of the μ's. The force γ_{LS} will be made up of the components γ_{Ls} and γ_{Sl}, the latter being the force in the liquid surface layer of the solid necessary to ensure equality of the μ's of atoms in surface layer and interior.

§ 5. SURFACE ENERGY AND SURFACE TENSION

Writers on the fundamentals of surface phenomena usually stress the equivalence of surface tension and surface energy and some writers regard the terms as synonymous. The use of these terms is here discussed in the light of the ideas of the preceding section.

The Helmholtz free energy of a surface is the maximum work which can be obtained when the surface is annihilated at constant temperature. This is equal to one half of the work of cohesion. We have seen that there are forces in the planes of the surfaces of solids with non-migratory atoms (induced forces) but that these are not equal to one half of the work of cohesion. To use surface tension as synonymous with surface energy is therefore clearly inadmissible.

In the case of surfaces of liquids and of solids with migratory atoms, if the atoms are exceedingly mobile so that there is no delay in attaining thermal equilibrium after the surface has been formed, then surface tension and surface energy are equivalent provided the latter is understood to be the Helmholtz free energy. If a surface is formed by brittle fracture in a very viscous liquid such as pitch or glass, the surface will be formed before the atomic migrations, which cause the equilibrium tension to be set up in the surface, can take place. If we limit ourselves to events taking place in a short time the considerations already discussed regarding solids with non-migratory atoms apply. If, however, we are interested in a longer period of time, migration of atoms will take place until thermal equilibrium is set up. The final force in the surface will not now be equal to the induced force, but it will be that necessary to ensure the equality of the μ's of surface and interior molecules. The migration of atoms which takes place in order that the system shall reach thermal equilibrium is an irreversible process and the Helmholtz free energy of the system is therefore decreased. It follows that a surface with a tension other than the tension necessary for thermal equilibrium has excess Helmholtz free energy. This can be estimated by calculating what work could be obtained from the surface by operations involving only reversible processes. Let the equilibrium surface tension be γ_e and the tension in the surface whose Holmholtz free energy it is desired to calculate be γ_0 and let its area be A_0. Then we may, by altering the external forces, cause the surface to alter its area elastically and reversibly until the surface tension equals γ_e, the operation being supposed to be sufficiently slow to be isothermal but sufficiently rapid for no appreciable migration of atoms to take place. The work done on the surroundings during the elastic alteration in surface area is equal to

$$\int_{A_e}^{A_0} \gamma \, dA,$$

where A_e is the area at which the tension equals γ_e. The surface now has its equilibrium tension and its Helmholtz free energy is $\gamma_e A_e$. The initial free energy was therefore

$$\gamma_e A_e + \int_{A_e}^{A_0} \gamma \, dA.$$

The free energy of a surface having the initial area but the equilibrium value of the tension would be $\gamma_e A_0$. The excess free energy of a surface having initial tension γ_0 is thus

$$\gamma_e A_e + \int_{A_e}^{A_0} \gamma \, dA - \gamma_e A_0 = (\gamma_0 - \gamma_e) A_0 + \int_{\gamma_0}^{\gamma_e} A \, d\gamma.$$

If we assume a linear relationship between area and tension when the number of molecules in the surface is constant the difference can be computed in terms of the effective elastic constant E_1 of the surface. If the initial tension is zero, the fractional excess free energy is $\gamma_e/2E_1$. An estimate of E_1 can be obtained from the bulk modulus K of the liquid by means of the relationship

$$E_1 = \frac{3(1-2\sigma)}{2(1-\sigma)}\,Kt,$$

where σ is Poisson's ratio and t the effective thickness of the surface layer. Assuming σ to be 1/3 and t to be equal to the cube root of the volume per molecule, the value of $\gamma_e/2E_1$ for some common liquids such as water, benzene and mercury is of the order of 5%.

REFERENCES

Brown, R. C., 1947, *Proc. Phys. Soc.*, **59**, 429.
Chalmers, B., King, R., and Shuttleworth, R., 1948, *Proc. Roy. Soc.* A, **193**, 465.
Frenkel, J., 1945, *J. Phys. U.S.S.R.*, **9**, 392.
Gibbs, J. W., 1876, *Collected Works* (New York : Longmans, 1928).
Gurney, C., 1947, *Nature, Lond.*, **160**, 166.
Kelvin, Lord, 1886, *Popular Lectures and Addresses*, Vol. 1, 1891.
Laplace, P. S.. 1807, *Mécanique céleste*, Bk. IV, Supplement, Paris.
Lennard-Jones, J. E., and Dent, B. M., 1928, *Proc. Roy. Soc.* A, **121**, 256.
Pauling, J., 1940, *The Nature of the Chemical Bond*, 2nd Edition (New York : Corner University Press).
Young, T., 1805, *Phil. Trans. Roy. Soc.*, **27**, 67.

The Hydrodynamics of Helium II

By R. B. DINGLE
Royal Society Mond Laboratory, Cambridge

Communicated by H. N. V. Temperley; MS. received 29th April 1949

ABSTRACT. In this paper expressions are derived for the forces acting on the normal fluid and on the superfluid of helium II, and it is shown that the apparently differing derivations of the velocity of second sound given by Landau and Tisza are, in fact, equivalent, even if thermal expansion is not neglected.

§ 1. INTRODUCTION

In discussing the properties of helium II from a phenomenological standpoint it is customary to suppose that the fluid may be considered as some type of mixture of two phases, the normal fluid and the superfluid. The superfluid is assumed to carry little or no entropy, and to be entirely non-viscous. These assumptions are displayed quantitatively as follows. Let ρ be the density of the fluid as a whole, ρ_n that of the normal fluid, and ρ_s that of the superfluid. Then $\rho=\rho_n+\rho_s$. Let $\dot{x}_n$ and $\dot{x}_s$ be the velocities of the normal and superfluid respectively, so that the current j is given by $j=\rho_n\dot{x}_n+\rho_s\dot{x}_s$. Finally, let T, p and t be the temperature, the pressure and the time respectively, and S the entropy of the fluid considered as a whole. In this notation, Landau (1941) proposed the following equations to describe the hydrodynamics of helium II to the first order*:

$$\partial p/\partial t+\nabla . j=0, \qquad \ldots\ldots(1)$$

$$\partial(\rho S)/\partial t+\rho S\nabla . \dot{x}_{\mathrm{n}}=0, \qquad \ldots\ldots(2)$$

$$\partial j/\partial t+\nabla p=0, \qquad \ldots\ldots(3)$$

$$\partial \dot{x}_{\mathrm{s}}/\partial t-S\nabla T+\nabla p/\rho=0. \qquad \ldots\ldots(4)$$

Equation (1) expresses the conservation of mass, equation (2) the conservation of entropy in a system in which the entropy is transported by the normal fluid only, and equation (3) is the usual kinematical equation giving the acceleration of the bulk fluid in terms of the mechanical force. The fourth equation was derived by Landau from a thermodynamical argument showing that the force acting on unit volume of the superfluid considered alone is given by the gradient of the thermodynamical potential. There appears to be some reluctance to accept equation (4) on the same standing as equations (1), (2) and (3) (see for instance London and Zilsel 1948), apparently on account of the fact that it introduces a new kind of force, a thermal pressure proportional to the temperature at the plane considered.

With the aid of these equations, Landau deduced an approximate expression (neglecting the coefficient of thermal expansion) for the velocity of second sound, and Lifshitz (1944) examined the ratio of the amplitudes of first and second sound produced by various forms of excitation. Approaching the problem from a different standpoint, and assuming the conservation equations (1) and (2), but not the kinematical equations (3) and (4), Tisza (1947) has deduced the same approximate expression for the velocity of second sound.

In this paper we shall deduce Landau's equations (3) and (4), together with further similar equations, by differentiation of a Lagrangian of the complete system similar to that given by Tisza. Hence the Tisza and Landau formulations are equivalent. This equivalence holds even if the coefficient of thermal expansion is not neglected. The work contained in this paper, and in a previous paper by the author (Dingle 1948), shows that it is unnecessary to introduce the concept of "osmotic pressure" as Tisza does, thereby avoiding his assumption† that $\rho_{\mathrm{n}} \propto S$. Again, the fact that the equivalence holds even if thermal expansion is not neglected shows that it is unnecessary to repeat (on Tisza's theory) Lifshitz's calculations on the amplitude ratio of first and second sound produced by various processes. The present work shows also that Landau's equation (4), which was deduced assuming perfect reversibility, would still hold, at least approximately, if irreversible processes took place.

As is shown in this paper, (3) and (4) may be derived thermodynamically if we assume the validity of (1) and (2). Since (1) merely expresses the conservation of mass, the only serious assumption of the hydrodynamical theory is contained in (2), which expresses the fact that the entropy is transported only by the normal fluid. This assumption is well-founded experimentally.

---

* Quadratic terms are omitted. Thus we neglect the difference between full and partial differentiation with respect to the time (the difference being quadratic in the velocities), and in products such as $\rho_{\mathrm{n}}\dot{x}_{\mathrm{n}}$ we ignore the variation of ρ_{n}.

† This assumption has been criticized by Dingle (1948) and by Landau (1949), who implies that the whole of Tisza's quantitative theory is incorrect as a result. The present author believes that the proportionality is probably correct for those adiabatic changes in which relaxation effects are negligible.

§ 2. THE POTENTIAL ENERGY OF THE SYSTEM

For the sake of completeness*, we shall first give the calculation of the potential energy of unit mass of a part of the fluid having excess entropy δS and excess volume δV. Let us suppose that the unit mass forms a sub-system immersed in a surrounding medium at constant temperature T_0 and constant pressure p_0, the sub-system and the surrounding medium together forming an isolated system.

The work done by the medium on the sub-system is $p_0 \delta V_0$, and the heat transferred is $-T_0 \delta S_0$. Let the internal energy change of the sub-system be δU, and the work done on the sub-system by a source of work be δW. Then, by the first law of thermodynamics, $T_0 \delta S_0 = p_0 \delta V_0 - \delta U + \delta W$.

The physical meaning of the ideal processes described may be seen more clearly if we imagine the sub-system to consist of a cylinder fitted with a piston which is always impermeable to normal fluid, but which may be made either permeable or impermeable to superfluid. Neglecting thermal expansion, we alter only the volume per unit mass if the piston is moved whilst impermeable to superfluid, and only the entropy per unit mass if it is moved whilst permeable. δW is the work required to move the piston.

The volume of the whole (medium plus sub-system) will be constant; hence $\delta V_0 = -\delta V$. Now the entropy of the whole must either remain constant—perfect reversibility—or increase; thus $\delta S_0 \geqslant -\delta S$. Assuming perfect reversibility for the present, we have $\delta W + T_0 \delta S - p_0 \delta V = \delta U$. Expanding δU in terms of the values appropriate to the surrounding medium, we have

$$\begin{aligned}\delta U = \left(\frac{\partial U}{\partial V}\right)_{0S} \delta V + \left(\frac{\partial U}{\partial S}\right)_{0V} \delta S + \frac{1}{2}\left(\frac{\partial^2 U}{\partial V^2}\right)_{0S} \delta V^2 \\ + \left(\frac{\partial^2 U}{\partial V \partial S}\right)_{0} \delta V \delta S + \frac{1}{2}\left(\frac{\partial^2 U}{\partial S^2}\right)_{0V} \delta S^2 \ldots . \\ = -p_0 \delta V + T_0 \delta S - \frac{1}{2}\left(\frac{\partial p}{\partial V}\right)_{0S} \delta V^2 - \left(\frac{\partial p}{\partial S}\right)_{0V} \delta V \delta S + \frac{1}{2}\left(\frac{\partial T}{\partial S}\right)_{0V} \delta S^2 \ldots .\end{aligned}$$

Hence
$$\delta W = -\frac{1}{2}\left(\frac{\partial p}{\partial V}\right)_{0S} \delta V^2 - \left(\frac{\partial p}{\partial S}\right)_{0V} \delta V \delta S + \frac{1}{2}\left(\frac{\partial T}{\partial S}\right)_{0V} \delta S^2. \quad \ldots\ldots (5)$$

δW is the work done on the sub-system by the source of work necessary to increase its entropy and its volume above their equilibrium values by amounts δS and δV respectively; i.e. it is the potential energy per unit mass. The derivatives of this energy (taken with a negative sign) will be proportional to the forces called into play. When only the density changes, the force will be entirely mechanical, being proportional to

$$-\left(\frac{\partial\, \delta W}{\partial\, \delta V}\right)_{\delta S} = \left(\frac{\partial p}{\partial V}\right)_{S} \delta V + \left(\frac{\partial p}{\partial S}\right)_{V} \delta S = \delta p, \quad \ldots\ldots (6)$$

a remarkably simple result. On the other hand, when only the entropy changes, the force will be entirely thermal, proportional to

$$-\left(\frac{\partial\, \delta W}{\partial\, \delta S}\right)_{\delta V} = \left(\frac{\partial p}{\partial S}\right)_{V} \delta V - \left(\frac{\partial T}{\partial S}\right)_{V} \delta S = -\delta T, \quad \ldots\ldots (7)$$

since
$$\left(\frac{\partial p}{\partial S}\right)_{V} = -\frac{\partial}{\partial S}\left(\frac{\partial U}{\partial V}\right) = -\frac{\partial}{\partial V}\left(\frac{\partial U}{\partial S}\right) = -\left(\frac{\partial T}{\partial V}\right)_{S}.$$

---

* Cf. Landau, L., and Lifshitz, E., *Statistical Physics* (Oxford: University Press).

§3. MECHANICAL AND THERMAL FORCES

For the sake of symmetry and generality we shall assume that the superfluid has a small but definite entropy S_s, that of the normal fluid being S_n. Then the measured entropy of the bulk fluid, S, is given by $\rho S = \rho_n S_n + \rho_s S_s$. Let x_n and x_s be vectors representing the displacements of normal and superfluid respectively. We introduce new coordinates x and y such that

$$\rho x = \rho_n x_n + \rho_s x_s, \qquad \ldots\ldots(8)$$

and

$$y = (\rho_n x_n S_n + \rho_s x_s S_s)/(\rho_n S_n + \rho_s S_s) - x. \qquad \ldots\ldots(9)$$

y is defined as the sum of the weighted displacements of the normal and superfluid relative to x, the displacement of the fluid as a whole. This weighting is taken as proportional to the entropy carried. Thus in these new coordinates the equation of conservation of entropy may be expressed in the simple form

$$\delta S/S + \nabla . y = 0. \qquad \ldots\ldots(10)$$

Also, in these coordinates, the equation of conservation of mass becomes

$$\delta\rho/\rho + \nabla . x = 0,$$

i.e.

$$\delta V/V - \nabla . x = 0. \qquad \ldots\ldots(11)$$

After some reduction, using the fact that $\rho = \rho_n + \rho_s$, we obtain for y

$$S\rho^2 y = \rho_n \rho_s S^*(x_n - x_s), \qquad \ldots\ldots(12)$$

where $S^* = S_n - S_s$. From these equations we obtain x_n and x_s in terms of x and y as follows:

$$x_n = x + y\rho S/\rho_n S^*, \qquad \ldots\ldots(13)$$

and

$$x_s = x - y\rho S/\rho_s S^*. \qquad \ldots\ldots(14)$$

Alternatively, relations (10) and (11) may be deduced analytically in the following way. The total entropy per unit volume ρS changes with time only by flow through the sides of the volume, the contribution $\rho_n S_n$ flowing with velocity $\dot{x}_n$, and the contribution $\rho_s S_s$ with velocity $\dot{x}_s$. Then, ignoring quadratic effects,

$$0 = \frac{\partial(\rho S)}{\partial t} + \rho_n S_n \nabla . \dot{x}_n + \rho_s S_s \nabla . \dot{x}_s$$

$$= S\left\{\frac{\partial\rho}{\partial t} + \rho_n \nabla . \dot{x}_n + \rho_s \nabla . \dot{x}_s\right\} + \left\{\rho\frac{\partial S}{\partial t} - (S - S_n)\rho_n \nabla . \dot{x}_n - (S - S_s)\rho_s \nabla . \dot{x}_s\right\}.$$

The terms in the first bracket together give zero, since mass is conserved; integrating over time, $\delta\rho + \rho\nabla . x = 0$. Using the definition $\rho S = \rho_n S_n + \rho_s S_s$, we have

$$-\rho_n(S - S_n) = \rho_s(S - S_s) = \rho_s \rho_n S^*/\rho,$$

where $S^* = S_n - S_s$. Thus the terms in the second bracket give

$$\frac{\partial S}{\partial t} + \frac{\rho_s \rho_n}{\rho^2} S^* \nabla . (\dot{x}_n - \dot{x}_s) = 0.$$

Integrating over time, we obtain

$$\delta S + S\nabla . y = 0,$$

where y is defined by (12).

Since the coordinate x gives the position of the centre of gravity of the normal and superfluid, the conservation law (11) shows that the density changes on movement of the centre of gravity of the two fluids. Again, since the coordinate y is proportional to the relative displacement of the normal and the superfluid, the conservation law (10) shows that the entropy changes with the relative displacement of the two fluids.

The potential energy δW of the system may now be expressed simply in terms of $\nabla . x$ and $\nabla . y$ by using the conservation laws (10) and (11). The kinetic energy may be expressed in terms of $\dot{x}^2$ and $\dot{y}^2$ by means of (13) and (14). Then the velocities of first and second sound may be deduced from the Euler equations

$$\frac{d}{dt}\left(\frac{\partial L}{\partial \dot{x}}\right) - \frac{\partial L}{\partial x} = -\nabla\left(\frac{\partial L}{\partial \nabla . x}\right),$$

and

$$\frac{d}{dt}\left(\frac{\partial L}{\partial \dot{y}}\right) - \frac{\partial L}{\partial y} = -\nabla\left(\frac{\partial L}{\partial \nabla . y}\right),$$

where L is the Lagrangian of the system, formed by taking the difference between the kinetic and potential energies. The calculation in these coordinates has been previously given (Dingle 1948).

Combining (6) with the equation of mass conservation (11), we have

$$-\left(\frac{\partial\, \delta W}{\partial \nabla . x}\right)_y = -V\left(\frac{\partial\, \delta W}{\partial\, \delta V}\right)_S = V\delta p, \qquad \ldots\ldots(15)$$

giving the mechanical force acting on unit mass of the fluid when it is displaced as a whole.

Combining (7) with the equation of entropy conservation (10), we have

$$-\left(\frac{\partial\, \delta W}{\partial \nabla . y}\right)_x = S\left(\frac{\partial\, \delta W}{\partial\, \delta S}\right)_V = S\delta T, \qquad \ldots\ldots(16)$$

giving the thermal force acting on unit mass of the fluid when normal and superfluid are displaced in such a way that the fluid considered as a whole remains at rest.

§ 4. FORCES ACTING ON THE FLUID

(i) *The Force acting on the Superfluid alone*

We wish to calculate the force acting on the superfluid when this alone is displaced, i.e. the value of $-(\partial\, \delta W/\partial \nabla . x_s)_{x_n}$. Now from (8) and (12) we have $(\partial x/\partial x_s)_{x_n} = \rho_s/\rho$ and $(\partial y/\partial x_s)_{x_n} = -\rho_n\rho_s S^*/\rho^2 S$. Then

$$\left(\frac{\partial\, \delta W}{\partial \nabla . x_s}\right)_{x_n} = \frac{\partial\, \delta W}{\partial \nabla . x} \cdot \left(\frac{\partial x}{\partial x_s}\right)_{x_n} + \frac{\partial\, \delta W}{\partial \nabla . y} \cdot \left(\frac{\partial y}{\partial x_s}\right)_{x_n}$$

$$= -\frac{\rho_s}{\rho} V\delta p + \frac{\rho_n\rho_s}{\rho^2} S^*\delta T$$

by (15) and (16). Hence the resultant force acting on unit volume of the fluid is

$$\rho_s \frac{d\dot{x}_s}{dt} = -\rho\nabla\left(-\frac{\partial\delta W}{\partial \nabla . x_s}\right)_{x_n} = \rho_s\left(-\frac{\nabla p}{\rho} + \frac{\rho_n}{\rho} S^*\nabla T\right). \qquad \ldots\ldots(17)$$

The force is therefore partly mechanical and partly thermal.

(ii) *The Force acting on the Normal Fluid alone*

We have, similarly,

$$\left(\frac{\partial\,\delta W}{\partial\,\nabla.x_{\rm n}}\right)_{x_{\rm s}}=\frac{\partial\,\delta W}{\partial\,\nabla.x}\left(\frac{\partial x}{\partial x_{\rm n}}\right)_{x_{\rm s}}+\frac{\partial\,\delta W}{\partial\,\nabla.y}\left(\frac{\partial y}{\partial x_{\rm n}}\right)_{x_{\rm s}}$$

$$=-\frac{\rho_{\rm n}}{\rho}V\delta p-\frac{\rho_{\rm n}\rho_{\rm s}}{\rho^2}S^*\delta T.$$

Hence the resultant force per unit volume of fluid is

$$\rho_{\rm n}\frac{d\dot{x}_{\rm n}}{dt}=-\rho\nabla\left(-\frac{\partial\,\delta W}{\partial\,\nabla.x_{\rm n}}\right)_{x_{\rm s}}=\rho_{\rm n}\left(-\frac{\nabla p}{\rho}-\frac{\rho_{\rm s}}{\rho_{\rm n}}S^*\nabla T\right).\quad\ldots\ldots(18)$$

The force is again partly mechanical and partly thermal. Equation (18) is important, as it gives directly the force driving the heat current $\rho ST_0\dot{x}_{\rm n}$.

(iii) *The Force opposing Relative Displacement of Normal and Superfluid*

The force tending to restore equilibrium when the normal and superfluid are displaced relatively to each other will be entirely thermal, since by (12)

$$\frac{\partial\,\delta W}{\partial\,\nabla.(x_{\rm n}-x_{\rm s})}=\frac{\rho_{\rm n}\rho_{\rm s}S^*}{\rho^2 S}\frac{\partial\,\delta W}{\partial\,\nabla y}=-\frac{\rho_{\rm n}\rho_{\rm s}S^*}{\rho^2}\delta T,\qquad\ldots\ldots(19)$$

by (16).

(iv) *Action of the Mechanical Force*

Adding equations (17) and (18), and neglecting quadratic terms, we have

$$\partial j/\partial t+\nabla p=0,\qquad\ldots\ldots(20)$$

since $\rho=\rho_{\rm n}+\rho_{\rm s}$ and $j=\rho_{\rm n}\dot{x}_{\rm n}+\rho_{\rm s}\dot{x}_{\rm s}$ by definition. Thus the mechanical force acts on the total current j. This confirms Landau's equation, (3) of this paper.

(v) *Action of the Thermal Force*

We shall now confirm the proposition that the thermal force acts only in restoring the relative displacement of the normal and superfluid to its equilibrium value zero, a result suggested by (19). We have, from (17),

$$\frac{d}{dt}\dot{x}_{\rm s}=-\frac{1}{\rho}\nabla p+\frac{\rho_{\rm n}}{\rho}S^*\nabla T,$$

and from (18)

$$\frac{d}{dt}\dot{x}_{\rm n}=-\frac{1}{\rho}\nabla p-\frac{\rho_{\rm s}}{\rho}S^*\nabla T.$$

Eliminating the mechanical force, we obtain

$$\frac{d}{dt}(\dot{x}_{\rm n}-\dot{x}_{\rm s})=-S^*\nabla T.\qquad\ldots\ldots(21)$$

Thus the thermal force acts on the relative velocity of normal and superfluid.

§ 5. CASE WHEN THE SUPERFLUID HAS ZERO ENTROPY

When the entropy of the superfluid is neglected, we usually associate the entropy with the bulk fluid considered as a whole. Then $S^* = S_n - S_s = \rho S/\rho_n$. In this case, (17) reduces to

$$\frac{d\dot{x}_s}{dt} = -\frac{1}{\rho}\nabla p + S\nabla T, \qquad \ldots\ldots(22)$$

which is Landau's equation, (4) of this paper, quadratic terms being neglected. Similarly, (18) reduces to

$$\frac{d\dot{x}_n}{dt} = -\frac{1}{\rho}\nabla p - \frac{\rho_s}{\rho_n} S\nabla T, \qquad \ldots\ldots(23)$$

giving the acceleration of the heat current.

§ 6. IRREVERSIBILITIES

The expression (5) for the potential energy of the system was deduced for a reversible process, i.e. for one in which the entropy of the whole system (subsystem plus medium) remains constant. If the entropy increases due to some irreversibility, we must add to the right-hand side of (5) terms of the form $T_0 \delta S_{\text{irrev}}$. In addition, irreversible processes will alter the form of the equation of entropy conservation. We shall discuss two types of irreversibility, that due to ordinary thermal conduction and that due to viscous effects.

(i) *Ordinary Thermal Conduction*

In this case the maximum irreversible gain of entropy per unit volume is given by $\delta Q/T_0 = -K\nabla^2 T \,.\, \delta t/T_0$, where K is the ordinary heat conductivity, not involving movement of the fluid. Hence we must add a term of the form $-K\nabla^2 T\delta t$ to the right-hand side of (5), δt being the change in time. The partial differential coefficients with respect to δV and δS do not involve the time, so that the forces, both thermal and mechanical, retain the values already given. However, the equation of entropy conservation must be written as

$$\frac{\partial(\rho S)}{\partial t} + \rho S \nabla \,.\, \dot{x}_n - \frac{K}{T_0}\nabla^2 T = 0. \qquad \ldots\ldots(24)$$

The consequences of this change have been discussed in a previous paper (Dingle 1948).

(ii) *Viscous Effects*

The dissipation function per unit volume due to the viscosity μ of the normal fluid is given by (cf. Rayleigh 1926)

$$\mu\left[\left(\frac{\partial \dot{x}_{nu}}{\partial u}\right)^2 + \left(\frac{\partial \dot{x}_{nv}}{\partial v}\right)^2 + \left(\frac{\partial \dot{x}_{nw}}{\partial w}\right)^2 - \tfrac{2}{3}(\nabla \,.\, \dot{x}_n)^2 + \tfrac{1}{2}\left(\frac{\partial \dot{x}_{nv}}{\partial w} + \frac{\partial \dot{x}_{nw}}{\partial v}\right)^2 \right.$$
$$\left. + \tfrac{1}{2}\left(\frac{\partial \dot{x}_{nw}}{\partial u} + \frac{\partial \dot{x}_{nv}}{\partial w}\right)^2 + \tfrac{1}{2}\left(\frac{\partial \dot{x}_{nu}}{\partial v} + \frac{\partial \dot{x}_{nv}}{\partial u}\right)^2\right], \qquad \ldots\ldots(25)$$

where u, v, and w are three Cartesian coordinates.

On differentiation with respect to $\dot{x}_{\mathrm{n}}$, this gives rise to a force per unit volume of magnitude

$$\mu[\nabla^2\dot{x}_{\mathrm{n}}+\tfrac{1}{3}\nabla\nabla\,.\,\dot{x}_{\mathrm{n}}]=\mu[-\nabla\wedge(\nabla\wedge\dot{x}_{\mathrm{n}})+\tfrac{4}{3}\nabla\nabla\,.\,\dot{x}_{\mathrm{n}}]. \qquad \ldots\ldots(26)$$

This force acts on the normal fluid only, since the derivative of (25) with respect to $\dot{x}_{\mathrm{s}}$ vanishes.

The entropy gain to due this irreversible process is quadratic in the velocities, and may be neglected, leaving the equation of entropy conservation unchanged. Thus equation (17) (or (4)) for the force acting on the superfluid is unchanged, but equation (18) for the force acting on the normal fluid becomes

$$\rho_{\mathrm{n}}\frac{d\dot{x}_{\mathrm{n}}}{dt}=-\rho_{\mathrm{n}}\left(\frac{1}{\rho}\nabla p\mp\frac{\rho_{\mathrm{s}}}{\rho}S^*\nabla T\right)+\mu(\nabla^2\dot{x}_{\mathrm{n}}+\tfrac{1}{3}\nabla\nabla\,.\,\dot{x}_{\mathrm{n}}), \qquad \ldots\ldots(27)$$

and (20) becomes

$$\frac{\partial j}{\partial t}+\nabla p-\mu(\nabla^2\dot{x}_{\mathrm{n}}+\tfrac{1}{3}\nabla\nabla\,.\,\dot{x}_{\mathrm{n}})=0. \qquad \ldots\ldots(28)$$

REFERENCES

DINGLE, R. B., 1948, *Proc. Phys. Soc.*, **61,** 9.
LANDAU, L., 1941, *J. Phys. U.S.S.R.*, **5,** 71; 1949, *Phys. Rev.*, **75,** 884.
LIFSHITZ, E., 1944, *J. Phys. U.S.S.R.*, **8,** 110.
LONDON, F., and ZILSEL, P. R., 1948, *Phys. Rev.*, **74,** 1148.
RAYLEIGH, Lord, 1926, *Theory of Sound*, 2nd edition (London : Macmillan), p. 315.
TISZA, L., 1947, *Phys. Rev.*, **72,** 838.

The Dependence of the Thermal Diffusion Factor on Temperature

BY K. E. GREW
University College of the South-West, Exeter

Communicated by F. H. Newman; *MS. received* 18*th May* 1949

ABSTRACT. The thermal diffusion factor for isotopic mixtures has been calculated from values of the collision integrals given by Hirschfelder, Bird and Spotz which refer to molecules exerting an inverse 13th power repulsion with an inverse 7th power attraction—the (13, 7) model. The theoretical results are compared with experimental ones for the inert gas mixtures previously considered by Grew in relation to the (9, 5) model. The agreement is, as expected, better than for the (9, 5) model. Experimental results for hydrogen–helium mixtures are also given; the behaviour of these mixtures is exceptional in that the thermal diffusion factor appears to be independent of temperature over the range 12 to 600° K.

§ 1. INTRODUCTION

In the theory of transport phenomena in gases certain integrals involving the collision parameters occur. These integrals can be evaluated only by numerical methods, consequently the number of molecular models for which they are known is small. Recently Hirschfelder, Bird and Spotz (1948) have published results for a special case of the Lennard-Jones type of molecule. This is one whose force field is represented by an inverse power repulsion with a superposed inverse power attraction : thus the force between two molecules at distance r apart is

$$F=\kappa r^{-\nu}-\kappa' r^{-\nu'}$$

where κ, κ' are the force constants, ν, ν' the force indices, relating to the repulsive and the attractive force respectively. The case treated by Hirschfelder, Bird and Spotz is that in which the potential energy of interaction of two molecules separated by distance r is

$$E(r)=4\epsilon[(r_0/r)^{12}-(r_0/r)^6],$$

where r_0 is the separation for zero energy and ϵ is the minimum energy (taken as positive). The corresponding force indices are therefore 13 and 7. Hirschfelder, Bird and Spotz have discussed the viscosity and thermal conductivity of a gas composed of molecules of this type (as also have de Boer and v. Kranendonk 1948). In what follows, their results are applied to find the thermal diffusion factor as a function of temperature for this model, after which a comparison of the theoretical results with some experimental ones is made. A similar comparison for another case of the Lennard-Jones molecule, that in which $\nu=9$, $\nu'=5$, was made some time ago (Grew 1947); for this case the theoretical results are due to Clark Jones (1941).

§ 2. CALCULATION OF THE THERMAL DIFFUSION FACTOR

The Chapman–Enskog theory of non-uniform gases leads to the result that in a binary mixture in which a temperature gradient exists there is, in the steady state, a concentration gradient such that

$$\nabla n_{10}=-\nabla n_{20}=-\alpha n_{10}n_{20}\,.\,\nabla(\ln T),$$

where n_{10}, n_{20} are the proportionate numbers of the heavier (1) and lighter (2) molecules respectively, T is the temperature, and α is the thermal diffusion factor. The thermal diffusion factor in its first approximation may be expressed (following Chapman and Cowling's (1939) notation) as

$$[\alpha]_1=5(C-1)\frac{S_1n_{10}-S_2n_{20}}{Q_1n_{10}^2+Q_2n_{20}^2+Q_{12}n_{10}n_{20}},$$

where

$$S_1=M_1E_1-3M_2(M_2-M_1)-4M_1M_2A,$$

$$Q_1=E_1[6M_2^2+(5-4B)M_1^2+8M_1M_2A],$$

$$Q_{12}=3(M_1-M_2)^2(5-4B)+4M_1M_2A(11-4B)+2E_1E_2,$$

and S_2, Q_2 are derived from S_1, Q_1 by interchange of subscripts. Here

$$M_1=\frac{m_1}{m_1+m_2},\qquad M_2=\frac{m_2}{m_1+m_2},$$

m_1, m_2 being the masses of the two kinds of molecules. (M_1-M_2) is the proportionate mass difference, M. The quantities A, B, C, E_1, E_2 involve the collision integrals referred to above. These integrals are denoted in general by

$W^{(l)}(r)$, with subscript 1, 2 or 12 to distinguish the interactions of like and unlike molecules. Thus

$$A = \frac{W^{(2)}_{12}(2)}{5W^{(1)}_{12}(1)}, \qquad B = \frac{5W^{(1)}_{12}(2) - W^{(1)}_{12}(3)}{5W^{(1)}_{12}(1)}, \qquad C = \frac{2W^{(1)}_{12}(2)}{5W^{(1)}_{12}(1)},$$

$$E_1 = \frac{2A}{x_{12}(1-M)^{\frac{1}{2}}}, \qquad E_2 = \frac{2A}{x_{21}(1+M)^{\frac{1}{2}}},$$

where

$$x_{12} = \left(\frac{r_{0_{12}}}{r_{0_1}}\right)^2 \frac{W^{(2)}_{12}(2)}{W^{(2)}_{1}(2)}, \qquad x_{21} = \left(\frac{r_{0_{12}}}{r_{0_2}}\right)^2 \frac{W^{(2)}_{12}(2)}{W^{(2)}_{2}(2)}.$$

The integrals W can be evaluated, as Clark Jones showed in his original work for the (9, 5) model, for assigned values of the ratio $\boldsymbol{k}T/\epsilon$. The evaluation of $[\alpha]_1$ in the general (13, 7) case therefore requires a knowledge of the radii r_{0_1}, $r_{0_{12}}$, r_{0_2}, and the minimum values ϵ_1, ϵ_{12}, ϵ_2, of the energy. But for the isotopic case, in which there is no distinction between the (1, 1), (2, 2) and (1, 2) interactions, $x_{12} = x_{21} = 1$, and $[\alpha]_1$ may readily be found. This has been done for various values of the proportionate mass difference M, using the values of $W^{(l)}(r)$ tabulated by Hirschfelder, Bird and Spotz.

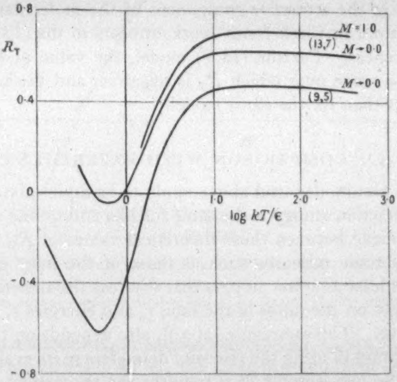

Figure 1. Values of the thermal separation ratio R_T as a function of $\boldsymbol{k}T/\epsilon$ for the (13, 7) model, and for the (9, 5) model.

From these values of $[\alpha]_1$ the thermal separation ratio R_T has been evaluated. This quantity was first introduced in the discussion of thermal diffusion experiments as a measure of the extent to which the molecular interactions approach the ideally hard ones of rigid spheres. Experimentally R_T is defined as the ratio of the thermal diffusion factor α, determined experimentally, to the calculated value (in first approximation) for molecules of the same mass and size as the experimental ones but interacting as rigid elastic spheres. Denoting this latter value by $[\alpha(\infty)]_1$,

$$R_T(\text{exp.}) = \alpha(\text{exp.})/[\alpha(\infty)]_1.$$

The molecular diameters are found by substitution of the experimental values of the viscosity in the theoretical expression for the viscosity of a gas consisting of rigid spheres. The corresponding theoretical quantity for a given molecular model is

$$R_T(\text{theor.}) = \alpha(\text{theor.})/[\alpha(\infty)]_1,$$

where α (theor.) is the calculated exact value of the thermal diffusion factor for that model. In the present case only the first approximation to α (theor.) is known, and the values of R_T (theor.) here considered are the ratios of the first approximations $[\alpha(13,7)]_1/[\alpha(\infty)]_1$. This approximate value is likely to be too small, but the error cannot be definitely stated. In the simpler case of molecules which behave as centres of repulsion only, however, an estimate of the error leads to the following values of the ratio of the exact value and the first approximation when $\nu = 13$:

M	0·1	0·5	0·7	1·0
$\alpha/[\alpha]_1$	1·03	1·10	1·13	1·18

The dependence of R_T on $\boldsymbol{k}T/\epsilon$ for this (13, 7) case is shown graphically in Figure 1, where the curves refer to the extreme values $M \to 0$ and $M = 1{\cdot}0$. The corresponding curve for the (9, 5) case, derived from Clark Jones' results, is also given. The marked dependence of R_T on the temperature (implying of course a similar dependence of the thermal diffusion factor) which results from the introduction of the attractive component of the molecular field, and which was first brought out in Clark Jones' work, appears in the (13, 7) case, but with interesting differences. For the (13, 7) model, the value of $\boldsymbol{k}T/\epsilon$ at which R_T changes sign, the range over which R_T is negative, and the minimum value of R_T are all smaller than for the (9, 5) model.

§ 3. COMPARISON WITH EXPERIMENT

Although the results deduced above apply to isotopic mixtures, that is those in which the interaction energy is the same for like and unlike molecules, a comparison may be made between these theoretical values of R_T and experimental values for non-isotopic mixtures such as those of the inert gases. The justification of this, at least as a first step, is that whereas the thermal diffusion factor α depends strongly on the ratios of the radii r_0 and energies ϵ, the value of R_T is much less sensitive. This is because $[\alpha(\infty)]_1$ also depends on these ratios, which are taken into account in using the viscosity diameters in its evaluation. A closer comparison in the non-isotopic case requires the theoretical values of α to be found using appropriate values of the three radii and minimum energies, quantities known in only some cases.

The inert gas mixtures.

The results of an investigation of thermal diffusion in mixtures of the inert gases have been described elsewhere (Grew 1947). A comparison was there made of the thermal separation ratio R_T determined experimentally in the range 90 to 600° K. with the theoretical values for the (9, 5) model calculated by Clark Jones (1941). In comparing these same results with the theoretical ones for the (13, 7) model the procedure followed previously has been slightly modified. As R_T is determined experimentally for a temperature T it is necessary to determine the corresponding value of $\boldsymbol{k}T/\epsilon$ before comparison with the theoretical values can be made. The appropriate value of ϵ to be used in the reduction has been taken as ϵ_{12}, the minimum energy of unlike molecules. This is a reasonable approximation because in the expression for $[\alpha]_1$ the factor which is strongly dependent on the temperature is $(C-1)$, and this involves the interaction energy of unlike molecules, and that only; the other factor varies but slightly with temperature. There are grounds for taking ϵ_{12} as the geometric mean of ϵ_1 and ϵ_2, the values appropriate to the interaction of like molecules; thus $\epsilon_{12}=(\epsilon_1\epsilon_2)^{\frac{1}{2}}$. ϵ_1 and ϵ_2 have been calculated from the relation, which for neon and argon at least has experimental justification (Fowler and Guggenheim 1939, p. 345): $\epsilon=\boldsymbol{k}T_c/1{\cdot}22$, where T_c is the critical temperature.

On this basis it is found that when the values of R_T for the nine different mixtures examined, after a small modification for the effect of the different mass ratios, are plotted against $\boldsymbol{k}T/\epsilon_{12}$, the curves are roughly superposable on a single curve. The mean values of R_T at various values of $\boldsymbol{k}T/\epsilon_{12}$ are shown in Figure 2. Except at the extreme values of $\boldsymbol{k}T/\epsilon_{12}$, the mean is found from values for, usually, four different mixtures. The deviations from the mean, which are indicated, are often considerable, but not so large as to suggest that the mixtures may not be considered as a group. Figure 2 shows also the theoretical values of R_T for an isotopic mixture in the (13, 7) case when $M=0{\cdot}7$, the value to which the experimental curves were adjusted before their mean was found.

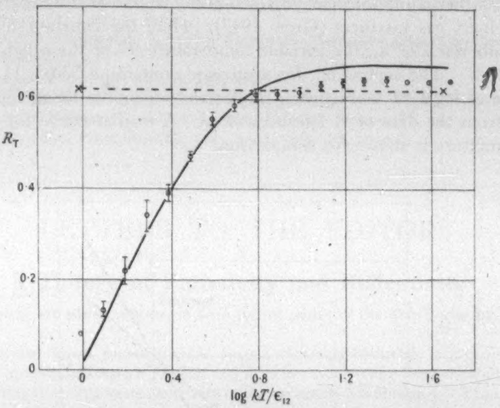

Figure 2. Full curve: values of R_T for (13, 7) model, with $M=0{\cdot}7$.
Φ : mean experimental values of R_T, with deviations, for the inert gas mixtures.
Broken curve: experimental values of R_T for the H_2–He mixtures.

It is clear that the (13, 7) model represents the experimental results much better that does the (9, 5) model, with which the previous comparison was made. There is an appreciable discrepancy at the higher temperatures, where the experimental error is relatively small. It is possible that this would not appear if the comparison were made with theoretical values of R_T calculated for a non-isotopic mixture. On the other hand the discrepancy may be larger than it appears here, for the theoretical values are first approximations to R_T, and if the error is comparable with that for molecules interacting as centres of repulsion only, the exact values may be perhaps 10 per cent greater.

Hydrogen–helium mixtures.

The behaviour of hydrogen–helium mixtures in thermal diffusion is of interest because it is to be expected that for these light molecules quantum mechanical effects may be apparent at low temperatures. Recently experimental measurements of the thermal diffusion effect in this and other mixtures have been reported by v. Itterbeek, v. Paemel and v. Lierde (1947). In this work the gas mixture was contained in a diffusion vessel consisting of two bulbs, the upper of which was at a fixed temperature T of 292° K., the lower at temperatures T' ranging from 90 to 12° K. The change of composition of the gas in the upper bulb resulting from thermal diffusion was determined from the viscosity change, and from this the separation, that is the difference in composition in the two bulbs, was found. The results for hydrogen–helium mixtures can be supplemented by others, hitherto unpublished, obtained in the course of the experimental work with the inert gas mixtures (Grew 1947). Here the constant temperature T of one bulb was 293° K., the variable temperature T' of the other ranged from 90 to 600° K. The separation, for a mixture containing 53·6% H_2 is shown as a function of $\log T'/T$ in Figure 3, the lower four points being found by interpolation from the data of v. Itterbeek *et al.* A similar curve for a hydrogen–nitrogen mixture is shown for comparison.

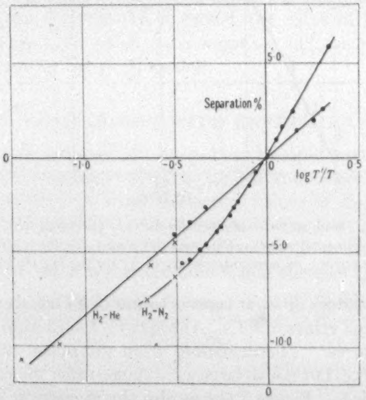

Figure 3. Separation as a function of $\log T'/T$ for H_2–He (53·6% H_2) and H_2–N_2 (39·8% H_2). × v. Itterbeek *et al.*; ● Grew.

The curve for the hydrogen–helium mixture is remarkable in being rectilinear over the whole range of T' from 12 to 600° K. This implies that the thermal diffusion factor α and the separation ratio R_T are independent of temperature in this range. All other mixtures so far examined behave like those of the inert gases in showing a decrease in R_T as the temperature falls. The value of R_T for this hydrogen–helium mixture is 0·59; if it is adjusted to correspond with $M=0{\cdot}7$ instead of the actual value $M=0{\cdot}33$, it becomes 0·62, and plotted with respect to $\boldsymbol{k}T/\epsilon_{12}$, as for the inert gas mixtures, it gives the curve shown in Figure 2.

Since R_T is independent of temperature, the interactions can be represented by an inverse power repulsion only. From theoretical values of R_T calculated for this case, the force index which, for an isotopic mixture, corresponds with $R_T = 0{\cdot}59$ when $M = 0{\cdot}33$ is found to be 11·3.

The thermal diffusion effect thus illustrates strikingly the abnormal behaviour of hydrogen and helium at low temperatures which is manifested in other ways. The apparent absence of an attractive component of the molecular field at temperatures so near the critical temperature is a point of considerable theoretical interest.

REFERENCES

de Boer, J., and v. Kranendonk, J., 1948, *Physica*, **14**, 442.

Chapman, S., 1940, *Proc. Roy. Soc.* A, **177**, 38.

Chapman, S., and Cowling, T. G., 1939, *Mathematical Theory of Non-uniform Gases* (Cambridge : University Press).

Fowler, R., and Guggenheim, A., 1939, *Statistical Thermodynamics* (Cambridge : University Press).

Grew, K. E., 1947, *Proc. Roy. Soc.* A, **189**, 402.

Hirschfelder, J. O., Bird, R., and Spotz, E. L., 1948, *J. Chem. Phys.*, **16**, 968.

v. Itterbeek, A., v. Paemel, O., and v. Lierde, J., 1947, *Physica*, **13**, 231.

Jones, R. Clark, 1940, *Phys. Rev.* **58**, 111 ; 1941, *Ibid.*, **59**, 1019.

LETTERS TO THE EDITOR

A Theory of Emissivity and Reflectivity

The following are some comments on a recent paper of the above title by D. J. Price (1949).

Dr. Price's manner of presenting the optical constants of metals is ingenious. Since the artifice he introduces is mathematical and does not contain any fundamentally new idea, it is not surprising that little agreement with experimental data is obtained. Thus he predicts a change of sign of the temperature coefficient of reflectivity in the region of transparency : but in a previous paragraph he puts the reflectivity R in that region equal to $\frac{1}{16}(\lambda/\lambda_0)^4$, which is clearly independent of the temperature. The intermediate region which is said to extend from $0{\cdot}1\,\mu$ to $10\,\mu$ is, according to his theory, characterized by a constant reflectivity. In effect, most metals show an increase in R which extends up to $3\,\mu$ if not more. The Hagen–Rubens approximation can, of course, be derived in a simpler manner. Dr. Price concludes from his failure to predict the observed temperature variation that either the influence of the bound electrons must be emphasized more strongly or a radical change in the theory of dispersion is required. Without some quantitative support such theorizing is unwarranted. Let it be said first of all that the Mott–Zener formulae (1934) describe the behaviour of most metals satisfactorily : the only drawback is that, in the visible, it is necessary to postulate the existence of surface layers of very high resistivity. This will be referred to below. Secondly, an X-point is inherent in the theory of dispersion as based on Maxwell's equations. This is easily seen if only one of the two Hagen–Rubens approximations is carried out. Then the emissivity E is given by

$$E = \frac{4\sqrt{\dfrac{\lambda}{\rho}}}{1 + 2\sqrt{\dfrac{\lambda}{\rho}} + 2\dfrac{\lambda}{\rho}}. \qquad \ldots\ldots(1)$$

When this is differentiated with respect to λ/ρ, E will be found to have a stationary value at

$$\lambda_X = \tfrac{1}{2}\rho. \qquad \ldots\ldots(2)$$

This is, of course, too short a wavelength as compared with experimental data. However, when the Mott–Zener theory is made the basis of the calculation (Weil 1948) it is found that

$$\lambda_X=\sqrt{3}\,\lambda_\tau, \qquad \ldots\ldots (3)$$

where $\lambda_\tau=2\pi c\tau$, and τ is twice the time of relaxation of the free electrons ($=m/\rho e^2 f_0$).

The writer has compiled a Table which compares calculated values of λ_X (the X-point of Price) with those found in the literature. Corrections have been carried out for the different temperature ranges covered by the various authors. At very high temperatures λ_X is practically constant since the temperature coefficient of resistivity becomes progressively smaller (cf. Ornstein's results). In this connection McCauley's data on tantalum are of interest. He refrained from " smoothing " his experimental curves, and the shift of λ_X in accordance with the above expression (3) is clearly seen. The agreement between the two sets of results is striking although they all occur in a transition region. No agreement could be obtained for copper, silver and gold.

It is seen that there is no need for an increased emphasis of the bound electrons. Nor is there any necessity radically to modify the theory of dispersion. This follows (*a*) from the agreement obtained above, and (*b*) from Kent's work (1919) on liquid metals. On the contrary, both (*a*) and (*b*) suggest that a large " Restwiderstand ", particularly obnoxious at medium temperatures, is responsible for the disagreement found between theory and experiment. It would appear to the writer that the only remedy lies in providing an improved technique for the preparation of mirrors : the development of anodic polishing is highly desirable from this point of view.

Comparison of calculated and observed values of λ_X (in μ)

	Ni	Pt	Pd	W	Mo	Ta	Fe	Steel
Calc.	1·6	2·51	2·99	4·32	5·5	1·9	2·43	—
Obs.	1) 1·8	4*a*) 0·7	4*b*) 1·0	5) 1·27	7) 1·4	4*c*) 0·8	8*a*) 1·0	8*b*) 1·0
Calc.	2·77	—	—	3·2	—	1·39	—	—
Obs.	2) 2·15	—	—	6) 1·65	—	4*d*) 0·6	—	9) 0·65
Calc.	2·1	—	—	—	—	—	—	—
Obs.	3) 2·5	—	—	—	—	—	—	—

In calculating the values of λ_X it is assumed that there is one free electron per atom.

	Mean temperature (°c.) covered by each author
1) Hurst, C., 1933, *Proc. Roy. Soc.* A, **142,** 466	925
2) Reid, C., 1941, *Phys. Rev.*, **60,** 161	470
3) Cennamo, F., 1939, *Atti accad. Italia*, **1,** 174	677
4) McCauley, G., 1913, *Astrophys. J.*, **37,** 164	(*a*) 1423
	(*b*) 1226
	(*c*) 1717
	(*d*) 2451
5) Weniger, G., and Pfund, A., 1919, *Phys. Rev.*, **14,** 427	1451
6) Ornstein, L. S., 1937, *Physica*, **3,** 561	2027
7) Price, D. J., 1947, *Proc. Phys. Soc.*, **59,** 131	1220
8) Hagen, E., and Rubens, H., 1910, *S.B. preuss. Akad. Wiss.*, **23,** 467	(*a*) 100
	(*b*) 85
9) Weil, R., 1947, *Nature, Lond.*, **159,** 305	100

Vision Research Unit,
Institute of Ophthalmology,
London W.C.1.

R. Weale.

Kent, C. V., 1919, *Phys. Rev.*, **14,** 459.
Mott, N. F., and Zener, H., 1934, *Proc. Camb. Phil. Soc.*, **30,** 249.
Price, D. J., 1949, *Proc. Phys. Soc.*, **62,** 278.
Weil, R., 1948, *Proc. Phys. Soc.*, **60,** 8.

AUTHOR'S REPLY

The dispersion equations and other physical assumptions used in this theory are identical in form with those employed by Mott, Krönig, Zener, and Mr. Weale himself. The removal of certain untractable expressions, and the examination of previous approximations shows that certain consequences of these usual assumptions are in greater conflict with experiment than had been supposed.

Bound electron effects are large in the intermediate region. This is evident in the case of silver, where the clearly differentiated resonance band affects the ordinary reflectivity curve so much that the lower limit of the intermediate region cannot occur before about $1{\cdot}0\,\mu$. This effect, together with the difficulty of accurate measurement, is probably the main reason why a large region of constant reflectivity has not been readily observed.

The excellent agreement obtained by Kent was, as stated, due to the use of a fundamentally different dispersion formula containing an extra term to take account of the bound electron contribution. His work therefore, far from supporting the present theory, is a further indication that some change is necessary.

The postulate of a surface layer having very different properties is widely used and attractive but, at the moment, it is a quite empirical device to reconcile theory and experiment.

The theory predicts that a zero value of the temperature coefficient of reflectivity can only occur near a region of transparency. As a matter of fact, the temperature coefficient is very near zero over the whole of the region of transparency of the model metal considered. There is no contradiction in this since, under such conditions, a true X-point cannot occur. Such phenomena, termed " spurious " X-points, have been noted in a previous paper (Price 1947).

The approximation from Maxwell's equations is not, of course, valid for so short a wavelength as the λ_X deduced from it.

Raffles College,
Singapore.

D. J. PRICE.

PRICE, D. J., 1947, *Proc. Phys. Soc.*, **59**, 131.

Hyperfine Splitting in Paramagnetic Resonance

Following the illness and sudden death of Dr. R. P. Penrose, after his discovery of the hyperfine structure in the paramagnetic absorption curve of a copper Tutton salt (Penrose 1949), we decided to investigate the behaviour of the hyperfine splitting of Cu^{++} in a similar way to that already undertaken for Co^{++} (Bleaney and Ingram 1949).

A crystal of $ZnSO_4\,(NH_4)_2SO_4\,6H_2O$ in which about one zinc ion in every 1,000 was replaced by a copper ion was investigated, using radiation of 3 cm. wavelength and at a temperature of 20° K. The procedure was analogous to that used for a systematic survey of the copper Tutton salts (Bleaney, Penrose and Plumpton 1949), except that the sensitivity of the apparatus was increased by modulating the applied D.C. magnetic field, and the amplified output is fed direct to an oscillograph screen, the time-base of this being fed from the modulating coils. In this way the absorption lines can be displayed directly on the screen provided the sweep of magnetic field is considerably larger than the line breadth.

By using the very dilute crystals the line width is so reduced that the hyperfine structure, due to the different orientations of the nucleus in the field of the electrons, can be resolved. The nuclear spin of both the copper isotopes is 3/2, and hence each electronic energy level is split into a further four levels, and for a selection rule $\Delta M=0$ four hyperfine lines should be obtained, M being the resolved component of I in direction of the field.

A systematic investigation of the variation of the splitting of these lines with orientation to the magnetic axes of the crystal has been undertaken. Like the corresponding cobalt salt (Bleaney and Ingram 1949), the crystal has two ions per unit cell with their tetragonal axes of electric field symmetry in the K_1K_3 plane. Measurements in this plane are of the most interest since maximum and minimum values of g and ΔH, the overall hyperfine splitting, are found parallel and perpendicular to a tetragonal axis.

The general results obtained are tabulated below, $\theta°$ being the angle of the applied magnetic field to the tetragonal axis ; and, as in the case of cobalt, it is found that $g^4(\Delta H)^2$ is a linear function of $\cos^2\theta$.

$\theta(°)$	ΔH	$g^4(\Delta H)^2 \times 10^5$	$\theta(°)$	ΔH	$g^4(\Delta H)^2 \times 10^5$
0	350	46·0	52	260	17·3
7	345	43·5	63	214	10·5
22	340	39·7	73	146	4·5
32	323	32·8	83	84	1·5
42	301	26·0	90	51	0·53

Two new features of interest arise in the study of this salt, however, namely the existence of an isotope splitting, and a splitting due to nuclear quadrapole moment.

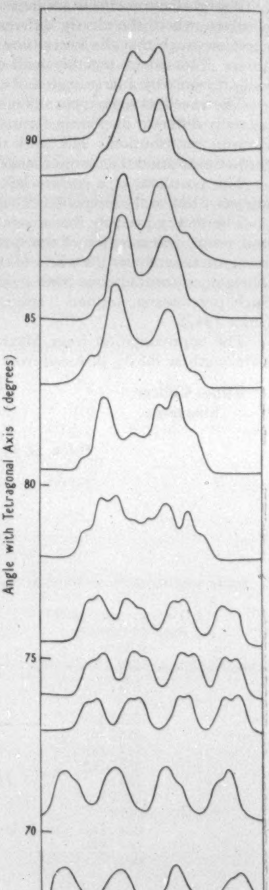

Figure 1.

At directions nearly parallel to a tetragonal axis the extreme lines of the hyperfine pattern are found to have a component of approximately half intensity partially separated on the outer sides. The two different isotopes of copper, of relative abundance 65 to 35, have a slightly different magnetic moment of ratio 1 to 1·071 (Pound 1948). Hence a splitting of $\frac{1}{2}\times 0{\cdot}07\times\Delta H$ would be expected, and for the maximum ΔH parallel to a tetragonal axis this is equal to 12 gauss. Experimentally the splitting is equal to 10 ± 2 gauss in this direction, and decreases as ΔH decreases; this therefore confirms the effect as due to the two different isotopes.

A very different effect occurs at a direction near the normal to a tetragonal axis, and the behaviour of the lines in this region is shown in Figure 1. As the angle increases from 60° to 80° each of the four lines is seen to split into two equal components of separation of the order of twelve gauss. The intensities of these appear to vary, however, and as the perpendicular direction is approached the whole pattern collapses as shown. By tracing individual lines through the pattern it would seem that a weak component first appears on the inner side of the original line, and that this gradually grows in intensity until it is about twice as strong as the latter.

This splitting is too large to be due to the isotope effect and appears to be caused by a combination of the magnetic interaction and the interaction of the nuclear electric quadrapole moment. Thus, near the tetragonal axis the magnetic effect dominates, but at angles nearly perpendicular to the axis this is weaker and the electric quadrapole moment becomes of the same order of magnitude; under these conditions the selection rule for ΔM breaks down, so that more than four lines are obtained.

On this assumption Professor Pryce has made some detailed calculations on the positions and intensities of the lines in the perpendicular direction. The results of this are shown in Figure 2, and are seen to agree quite well with the experimental curve.

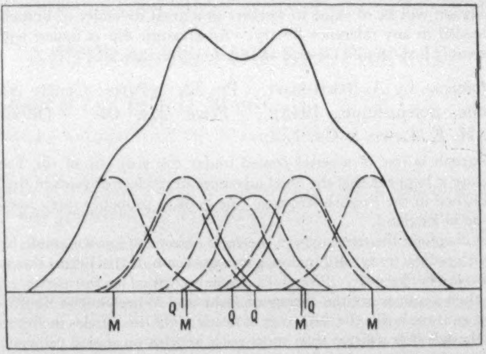

Figure 2. Theoretical prediction of line shape at $\theta=90°$.
M = line due to magnetic interaction. Q = line due to quadrapole interaction.

Measurements have also been made on dilute cobalt and copper fluosilicates. The hyperfine structure of the Co^{++} behaves similarly to the Tutton salt, g varying from 5·4 to 3·4 and ΔH from 520 to 193 gauss, parallel and perpendicular to the trigonal axis respectively, but the Cu^{++} now appears to have an isotropic g value.

I should like to thank Professor Pryce and Dr. Bleaney for much guidance whilst the experimental work was being performed.

Clarendon Laboratory,
Oxford.
4th July 1949.

D. J. E. INGRAM.

BLEANEY, B., and INGRAM, D. J. E., 1949, *Nature, Lond.*, **164**, 116.
BLEANEY, B., PENROSE, R. P., and PLUMPTON, B. I., 1949, *Proc. Roy. Soc.* A, in the press.
PENROSE, R. P., 1949, *Nature, Lond.*, **163**, 992.
POUND, R. V., 1948, *Phys. Rev.*, **73**, 523.

REVIEWS OF BOOKS

Compilation of Thermal Properties of Hydrogen in its Various Isotopic and Ortho-para Modifications, by H. W. WOOLLEY, R. B. SCOTT and F. G. BRICKWEDDE. Pp. 96. (U.S. Department of Commerce, National Bureau of Standards, 1948). 40 cents.

From spectra we learn the term levels and so may calculate the energies of the molecules of gas. The Boltzmann factors show how these will contribute to the physical properties, and so the entropy and free energy of a sufficiently rarefied gas may be calculated as functions of temperature and pressure. The properties of the real gas, at finite densities, are related to these properties for the rarefied (ideal) gas by thermodynamic formulae which involve the constants of the equation of state. Then such derived quantities as specific heat may be deduced in the familiar way.

The authors of this important monograph, which appears as Research Paper RP 1932 in volume 41 of the *Journal of Research of the National Bureau of Standards*, published in November 1948, have carried through this programme for hydrogen in its various forms. Starting with the spectroscopic data and applying statistical mechanics, they compute the thermodynamic functions from 10° K. to 2,000° K. for HD and D_2 and to 5,000° for H_2. They then tabulate pV/RT for the real gas as a function of temperature and density and so deduce the properties for the real gases. Ortho-para modifications and dissociation at high temperature are taken into account.

Other properties which do not follow so directly from basic data are also tabulated; they include viscosity and thermal conductivity, vapour pressure and the equation of state for the condensed phases. As far as data are available, tritium is included in all the fields surveyed.

The compilation will be of value to workers in a great diversity of branches of physics, and will be needed in any reference library. An erratum slip is issued with the reprint, and, since it is easily lost, should be used at once to correct the text. J. H. A.

Le Noyau atomique, by A. BERTHELOT. Pp. 32. (Paris: Centre National de la Recherche Scientifique, 1948). Price 25*s.* 6*d.* Obtainable from Messrs. H. K. Lewis & Co. Ltd.

This monograph is one of a series issued under the auspices of the French Physical Society. Because it happens that the chief advances in nuclear physics in the last few years have been published in the English language, the book is probably more needed in France than it would be in England.

Of its three chapters, the first surveys the facts about the known stable isotopes. The second deals with radioactivity, and includes an exposition of the Fermi theory, and a short account of Yukawa's field theory. The third chapter, entitled *nuclear fission*, rapidly surveys the facts, and then summarizes the theory of Bohr and Wheeler (the liquid-drop model).

The booklet as a whole fills the same sort of needs as do the articles in *Reports on Progress in Physics*; although it is shorter than most such articles on major subjects, it aims, like them, at helping physicists rather than laymen. It is very well written and, within its limits, is accurate and reliable. J. H. A.

RECENT PUBLICATIONS RECEIVED

How to Study Physics, by SEVILLE CHAPMAN. Pp. iv+28. Revised Edition. (Cambridge, Mass.: Addison-Wesley Press Inc., 1949.) 25 cents.

Die Brechzahlen einiger Halogenidkristalle, by H. HARTING. Pp. 25. Sitzungsberichte der Deutschen Akademie der Wissenschaften zu Berlin, Mathematische-Naturwissenschaftliche Klasse, Jahrgang 1948, Nr. IV. (Berlin: Akademie-Verlag, 1948.) 2.50 D.M.

Max Planck: In Seinen Akademie-Ansprachen (Erinnerungs-schrift der Deutschen Akademie der Wissenschaften zu Berlin). (Berlin: Akademie-Verlag, 1948.)

CONTENTS FOR SECTION B

PAGE
Prof. J. D. **Bernal**. The Physical Basis of Life 597
Mr. T. **Smith**. The Contributions of Thomas Young to Geometrical Optics, and their Application to Present-day Questions 619
Mr. R. J. **Donato**. The Diffuse Reflectivity of Oxide Layers Formed on Steels under Defined Conditions 629
Mr. H. **Ashcroft** and Dr. C. **Hurst**. Transit Time Correction Factor for Cylindrical Noise Diodes 639
Dr. W. I. **Pumphrey**. The Mode of Fracture at the Neck of a Tensile Specimen. 647
Dr. M. **McCaig**. The Magnetostriction of Anisotropic Permanent Magnet Alloys 652
Mr. W. **Hopwood**. The Positive Streamer Mechanism of Spark Breakdown . 657
Reviews of Books 664
Recent Publications Received 666
Contents for Section A 667
Abstracts for Section A 667

ABSTRACTS FOR SECTION B

The Physical Basis of Life, by J. D. Bernal.

32nd Guthrie Lecture, delivered 21st November 1947.

The Contributions of Thomas Young to Geometrical Optics, and their Application to Present-day Questions, by T. Smith.

ABSTRACT. Thomas Young's constructions for primary and secondary conjugate foci are described, and his algebraic equations are given. The latter are put into the form found most convenient when an instrument of several surfaces is considered. The special forms of these equations referred to the centres of curvature of the reflecting or refracting surfaces are used to show that in spherically symmetrical instruments the number of degrees of freedom—which is equal to the number of surfaces when these are spherical—must exceed the number of aberrations that can be corrected. It is concluded that non-spherical surfaces are likely to be very important, or perhaps essential, for any marked improvement in the correction of optical instruments, and that Young's equations, which relate expressly to spherical surfaces, may prove less useful in the future than they have been in the past.

The Diffuse Reflectivity of Oxide Layers Formed on Steels under Defined Conditions, by R. J. Donato.

ABSTRACT. A method to determine the reflectivity of oxide layers formed on steels under defined conditions at various wavelengths in the visible spectrum and at different temperatures up to 660° c. is described. An integrating sphere is used in which the specimen replaces a portion of the sphere wall, and a method is given for the simultaneous comparison of two beams of light using a single photocathode. Except for a correction factor depending upon the geometry of the sphere, the measurements rely solely upon the area of an adjustable aperture. Some results are given for the oxides of various steels.

Transit Time Correction Factor for Cylindrical Noise Diodes, by H. ASHCROFT and C. HURST.

ABSTRACT. The noise generated by a diode is always less than it would be if the transit of the electrons were instantaneous. The factor by which it is reduced has been evaluated for transit angles up to 12½ radians and for ratios of anode to cathode radius up to 20. It has been found to fall to zero for one pair of values of these parameters.

The Mode of Fracture at the Neck of a Tensile Specimen, by W. I. PUMPHREY.

ABSTRACT. Bridgman has shown that in a cylindrical specimen which is deforming plastically under longitudinal tension the tensile stress at the neck of the specimen is greatest on the longitudinal axis and least at the periphery of the specimen. Fracture therefore commences at the centre of the specimen and extends from the centre to the periphery. " Double-cup " fractures encountered during the tensile testing of a number of alloys at elevated temperatures have been accounted for in this way and an examination has been made of the metallurgical factors which govern the occurrence of this type of fracture.

The Magnetostriction of Anisotropic Permanent Magnet Alloys, by M. MCCAIG.

ABSTRACT. Blocks of permanent magnet alloys of the system Fe Ni Al Co Cu have been prepared with columnar crystals. The magnetostriction has been measured in various directions before and after heat treatment in a magnetic field. The results agree well with those predicted theoretically, and so confirm the postulated crystal structure.

The Positive Streamer Mechanism of Spark Breakdown, by W. HOPWOOD.

ABSTRACT. The essential conditions for streamer onset in spark breakdown are discussed, with particular reference to the production of photo-ionizing radiation in the initial avalanche. It is shown that the process of electron–ion recombination can adequately account for the production of the necessary radiation, and is probably the predominant process. It is also shown that the yield of photons by this mechanism, and consequently the threshold for streamer advance, is critically dependent upon the space-charge field produced by the initial avalanche. While Meek's criterion in its quantitative form gives the order of this critical space-charge field and enables the breakdown voltage for uniform electric fields to be calculated, the newly proposed conditions for photon production give a new physical significance to the criterion.